

## THERMONUCLEAR PROCESSES ON ACCRETING NEUTRON STARS: A SYSTEMATIC STUDY<sup>1</sup>

S. AYASLI<sup>2</sup> AND P. C. JOSS

Center for Space Research, Center for Theoretical Physics, and Department of Physics, Massachusetts Institute of Technology

*Received 1981 July 27; accepted 1981 October 22*

### ABSTRACT

We have carried out a series of model calculations for the evolution of the surface layers of an accreting neutron star. We systematically varied the neutron star mass, radius, core temperature, and surface magnetic field strength, as well as the accretion rate onto the neutron star surface and the metallicity of the accreting matter, in order to determine the effects of these parameters on the properties of thermonuclear flashes in the surface layers and the emitted X-ray bursts that result from such flashes. Our models take into account for the first time all of the following considerations: (1) We include all of the significant general relativistic corrections to the equations of stellar structure and evolution. (2) We introduce a simplified but adequate nuclear reaction network that takes into account proton-capture and alpha-capture reactions, as well as beta decays, involving nuclei with atomic masses up to  $A = 56$ . (3) We follow in detail the heat flow into and out of the neutron star core prior to and during a thermonuclear flash, in order to determine accurately the conditions required for the thermal equilibrium of the core.

Our principal conclusions are as follows: (1) The core temperatures required for thermal equilibrium are a factor of  $\sim 2$  lower than estimated in earlier work. The core temperatures are most strongly reduced at relatively high accretion rates ( $\gtrsim 10^{17} \text{ g s}^{-1}$ ) due to neutrino emission from the core, which is enhanced by general relativistic effects. However, the heat flow from the core still plays a significant role in determining the thermal structure of the surface layers prior to a thermonuclear flash. (2) Due to the effects of the gravitational redshift, the emitted X-ray bursts have lower peak luminosities and longer durations than those calculated in the Newtonian approximation. (3) The entrainment of hydrogen into helium flashes can cause the flashes to exhibit a rather wide range of observable effects and can decrease by a factor of several the ratio of persistent accretion-driven luminosity to time-averaged burst luminosity emitted by the neutron star. (4) The thermal inertia of the surface layers, the nuclear fuel left unburned by a flash, and the residual radioactivity of the flashed matter may be sufficient to cause substantial variations in the properties of successive X-ray bursts and the intervals between bursts.

The calculated bursts have properties that generally fall within the range of actual properties of observed type I cosmic X-ray bursts. Some of the most serious remaining discrepancies between the model calculations and the observational phenomena, such as the detection of peak luminosities in excess of the Eddington limit in a few burst sources, may be the result of effects of moderately strong surface magnetic fields that have not been fully included in the calculations. In particular, the suppression of radiative opacities by a strong field may be important in enhancing the peak luminosities. Although a number of theoretical and phenomenological questions remain unanswered, neutron star thermonuclear flashes continue to be a viable mechanism for producing type I X-ray bursts.

*Subject headings:* nuclear reactions — stars: accretion — stars: neutron — X-rays: bursts

<sup>1</sup>This work was supported in part by the National Science Foundation under grant AST78-21993 and by the National Aeronautics and Space Administration under grants NSG-7643 and NGL-22-009-638 and contracts NAS5-24441 and NAS8-27972.

<sup>2</sup>On leave from Middle East Technical University, Ankara, Turkey.

## I. INTRODUCTION

Thermonuclear flashes in the surface layers of accreting neutron stars have received increasing attention as a possible mechanism for producing cosmic X-ray bursts (see Lewin and Joss 1981 for a review). Following the initial suggestions by Woosley and Taam (1976) and Maraschi and Cavaliere (1977), various aspects of such flashes were investigated by Joss (1977), Lamb and Lamb (1978), Taam and Picklum (1978), Barranco, Buchler, and Livio (1980), Czerny and Jaroszyński (1980), Ergma and Tutukov (1980), Hōshi (1980), and Fujimoto, Hanawa, and Miyaji (1981). The results of detailed computations (Joss 1978; Taam and Picklum 1979; Joss and Li 1980; Taam 1980, 1981*a*) strengthen the conjecture that such flashes are responsible for X-ray bursts from most observed burst sources. Moreover, the theoretical work suggests that it may eventually be possible to obtain information on the fundamental properties (masses, radii, and so forth) of the underlying neutron stars from burst observations, especially in view of the probable importance of general relativistic effects in determining the properties of bursts (Goldman 1979; van Paradijs 1979). There remain, however, a number of theoretical and phenomenological problems in the interpretation of X-ray bursts as neutron-star thermonuclear flashes.

In this paper, we present the results of a new series of numerical computations of neutron star thermonuclear flashes. Our calculations include (i) all relevant general relativistic corrections to the equations of stellar structure and evolution, (ii) an approximate but adequate treatment of hydrogen-burning and helium-burning nuclear reactions involving nuclei with atomic masses up to  $A = 56$ , and (iii) a detailed treatment of the thermal balance of the neutron star core, including an accounting of the radiative and conductive heat flow into and out of the core and the neutrino losses from the core during a complete thermonuclear flash cycle. We also explore the influence of the neutron star mass, radius, core temperature, and surface magnetic field strength, the accretion rate, and the metallicity of the accreting matter upon the properties of the flashes.

In § II of this paper, we briefly describe the input physics and approximations that we utilize in our calculations, and we explain how the thermal balance of the neutron star core is calculated. In § III, we describe our technique for incorporating general relativistic corrections into the equations of stellar structure and evolution; our approximate procedure is remarkably simple but quite accurate, provided that the thickness of the region of interest (the freshly accreted envelope of the neutron star) is small compared to the neutron star radius. Our simplified nuclear reaction network, which includes the effects of proton-capture and alpha-capture reactions involving moderately heavy nuclei, is described in § IV.

Our numerical results are presented in § V. In § *Va* we describe our standard model, which assumes illustrative values for various parameters describing the neutron star and the accretion flow. In § *Vb* we present the results for a series of models wherein the accretion rate is varied over four orders of magnitude about the value assumed in the standard model. In § *V*, results are presented for a series of models wherein the core temperature is varied over an order of magnitude about the value assumed in the standard model, and we also give results for two models that explore the effects of variations in the accretion rate at very low and very high values of the core temperature. In § *Vd*, we present the results for several models wherein the neutron-star mass, radius, and magnetic field strength, as well as the initial metallicity of the accreting matter, are varied about their standard values. In § *Ve*, we explore a model in which all general relativistic corrections to the stellar structure and evolution equations are suppressed.

We discuss the results of our model calculations in § VI. In §§ *VIa*, *VIb*, and *VIc*, we discuss the heat balance of the neutron-star core, the impact of general relativistic effects upon our findings, and the importance of the approximations used in our nuclear reaction network, respectively. In § *VId*, we develop analytic criteria for the separation of the hydrogen-burning and helium-burning shells within the neutron star surface layers at low accretion rates and for the partial or complete suppression of thermonuclear flashes at high accretion rates, and we consider possible scaling relations to describe the results of numerical calculations. In § *VIe*, we discuss the importance of incomplete burning of nuclear fuel and residual radioactivity upon the properties of successive thermonuclear flashes, and in § *VI f* we consider the effects of strong surface magnetic fields upon nuclear processes in the surface layers. We conclude, in § VII, with a discussion of the most significant remaining difficulties in reconciling the thermonuclear flash model with the observed properties of type I cosmic X-ray burst sources.

## II. COMPUTATIONAL METHOD

We used a modified version of the stellar evolution code ASTRA (Rakavy, Shaviv, and Zinamon 1966, 1967) to calculate the evolution of the surface layers of accreting neutron stars. The basic code and earlier modifications were described by Joss (1978) and Joss and Li (1980). In this paper, we shall discuss only the major new modifications that we have incorporated.

The code was modified to take into account the general relativistic corrections to the equations of stellar structure and evolution (Thorne 1977 and references therein). We also took into account both hydrogen burning and helium burning by use of an expanded nuclear reaction network, based largely on work by Wallace and Woosley (1981), that includes twenty

nuclear species with atomic masses up to  $A = 56$ . These two major refinements in the code will be described in detail in §§ III and IV, respectively. Our third principal refinement is an improved treatment of the thermal balance of the neutron star core, which we describe below.

We calculate the evolution of the neutron star surface layers down to a density of  $\sim 10^7 \text{ g cm}^{-3}$ . We shall refer to the region beneath this level as the neutron star core, which we assume to be an incompressible sphere. Heat flows into or out of the core by radiative diffusion and thermal conduction across the interface with the surface layers. The core also loses heat by neutrino emission. The core will be in thermal equilibrium if the heat flow into the core during thermonuclear flashes (when the surface layers are relatively hot) is just balanced by the heat flow out of the core between flashes. This balance may be expressed as  $\bar{L}_{\gamma+c} + L_\nu = 0$ , where  $\bar{L}_{\gamma+c}$  is the sum of the time-averaged radiative and conductive luminosities from the core over a complete thermonuclear flash cycle and  $L_\nu$  is the neutrino luminosity of the core. (Due to the effects of the gravitational redshift, different observers will measure different values for the luminosities; in this section, we shall take all luminosities to be those measured by an observer at the neutron-star surface.) If the net heat flow into or out of the core changes (as might happen if, for example, the average accretion rate onto the neutron star varies), the thermal inertia of the core is such that the characteristic time scale for the resultant change in its thermal structure is  $\sim 10^2 - 10^3$  years (Lamb and Lamb 1978), which is much longer than the typical recurrence time ( $\lesssim 1$  day) between thermonuclear flashes. Hence, we are justified in taking the thermal structure and  $L_\nu$  to be constant throughout the calculation of a single thermonuclear flash cycle.

We have modified our computer code to track explicitly the heat flow into or out of the core during a flash cycle. This calculation enables us to estimate the conditions required for thermal equilibrium of the core with much higher accuracy than was heretofore possible (cf. Lamb and Lamb 1978; Joss 1978). In determining the heat flow, we take the temperature just inside the interface between the core and surface layers to have a fixed value throughout the evolutionary calculation. This assumption is justified by the high thermal inertia of the core, as described above. Moreover, due to the high thermal conductivity of the core (see Tsuruta 1979 for references), it is an adequate approximation to take the core to be isothermal, so that an observer on the neutron star surface sees the entire core to be at a single temperature,  $T_c$ . However, due to the effects of gravitational redshift, the temperature within the core as measured by local observers will be larger than  $T_c$  by a factor of  $(1+z)/(1+z_s)$ , where  $z$  and  $z_s$  are the redshifts (to infinity) from a point within the core and from the

surface, respectively (Glen and Sutherland 1980; Van Riper and Lamb 1981). (The redshift from any point within the surface layers is equal to  $z_s$ , since those layers have negligible total mass and are geometrically thin.)

From the temperature difference between the core and the inner edge of the surface layers, we directly calculated the instantaneous radiative plus conductive luminosity from the neutron star core,  $L_{\gamma+c}$ , at each time step of an evolutionary calculation. The value of  $\bar{L}_{\gamma+c}$  was then readily obtained from the behavior of  $L_{\gamma+c}$  during a complete thermonuclear flash cycle (i.e., from the onset of accretion to the end of the first flash, under the assumption that the recurrence times between flashes are all equal; see §§ VIc and VI d for a discussion). The value of  $L_\nu$  was estimated from the cooling calculations by Tsuruta (1979) for her neutron star model A, whose mass and radius are similar to those of our standard model (see § Va). In order to take into account the effects of gravitational redshift (see § III below), we modified Tsuruta's (1979) results in the following ways. (1) We assumed, for simplicity, that all neutrinos are emitted near the center of the star, and we took the local temperature at the center to be higher than that at the edge of the core by a factor of  $(1+z_c)/(1+z_s)$ , where  $z_c$  is the gravitational redshift from the center to infinity. (2) We took the neutrino luminosity at the neutron star surface to be lower than that emitted at the center by a factor of  $[(1+z_c)/(1+z_s)]^2$ . Utilizing these corrections, we obtained the following fit to Tsuruta's (1979) results:

$$L_\nu = 2.69 \times 10^{31} \left( \frac{T_0}{10^8 \text{ K}} \right)^6 \times \left[ 1 + 0.148 \left( \frac{T_0}{10^8 \text{ K}} \right)^2 \right] \left( \frac{1+z_c}{1+z_s} \right)^{-2} \text{ ergs s}^{-1}, \quad (1)$$

where

$$T_0 = \left( \frac{1+z_c}{1+z_s} \right) T_c.$$

The first term in square brackets in equation (1) represents bremsstrahlung neutrinos, and the second term represents neutrinos from the modified Urca processes.

We adopted  $(1+z_c)/(1+z_s) = 2.12$  from the calculations by Glen and Sutherland (1980) for a neutron star model (based on the Baym, Pethick, and Sutherland 1971 equation of state for nuclear matter) whose mass and radius are approximately equal to those of our standard model (see § Va). Since the neutron star mass ( $1.41 M_\odot$ ) is moderately high and the radius (6.57 km) is unusually small (due to the very soft nuclear-matter equation of state), the value of the factor  $(1+z_c)/(1+z_s)$  is exceptionally large, so that the central temperature

is exceptionally high. Hence, the value of  $L_\nu$  obtained from equation (1) with  $(1+z_c)/(1+z_s)=2.12$  represents a reasonable upper limit on the neutrino luminosity. We also considered the case  $L_\nu=0$  as an extreme lower limit to the neutrino luminosity.

For any given set of model parameters, the value of the quantity  $(\bar{L}_{\gamma+c} + L_\nu)$  during an evolutionary calculation can be obtained by the procedure described above. In principle, if values of  $(\bar{L}_{\gamma+c} + L_\nu)$  are obtained for two evolutionary calculations with different values of  $T_c$  but otherwise identical model parameters, then the value of  $T_c$  at which the neutron star core will be in thermal equilibrium can be estimated by interpolation. However, the highly nonlinear dependence of  $(\bar{L}_{\gamma+c} + L_\nu)$  upon  $T_c$  requires that the interpolation be treated carefully. For each interpolation that we carried out, we assumed a fitting formula for  $\bar{L}_{\gamma+c}$  of the form

$$\bar{L}_{\gamma+c} = \lambda T_c^{2.6} - \mu, \quad (2)$$

where  $\lambda$  and  $\mu$  are parameters to be fitted. The first term on the right-hand side of equation (2) represents the radiative and conductive heat loss from the neutron star core in the absence of nuclear burning in its surface layers; its dependence on  $T_c$  is taken from Tsuruta's (1979) results. The second term represents the time-averaged heat flow into the core due to nuclear burning; it will depend on various parameters (such as the accretion rate), but we assume that it is insensitive to the value of  $T_c$ .

For each pair of model calculations corresponding to different values of  $T_c$ , the values of  $\bar{L}_{\gamma+c}$  were evaluated and the parameters  $\lambda$  and  $\mu$  in equation (2) determined. The value of  $T_c$  at which the quantity  $(\bar{L}_{\gamma+c} + L_\nu)$  vanishes was then evaluated for each of our two illustrative expressions for  $L_\nu$  [i.e.,  $L_\nu=0$  and  $L_\nu$  given by eq. (1) with  $(1+z_c)/(1+z_s)=2.12$ ]. The results of these calculations will be presented and discussed in § VI a.

### III. GENERAL RELATIVISTIC CORRECTIONS

We have included in our calculations all of the relevant general relativistic corrections to the equations of stellar structure and evolution (Thorne 1977 and references therein), so that we are able to determine the effects of general relativity on neutron star thermonuclear flashes and their observable consequences. For the spherically symmetric and geometrically thin envelopes that we consider, it is possible to make some approximations that greatly simplify the requisite numerical calculations: (1) The densities and temperatures in the surface layers are sufficiently low that the gravitational effects of pressure and internal energy may be neglected. (2) The variation,  $\delta r$ , in the Schwarzschild radial coordinate,  $r$ , throughout the surface layers is small compared to the neutron star radius,  $R$ , and the variation,  $\delta m$ , in the gravitational mass,  $m$ , enclosed

within level  $r$  throughout the surface layers is small compared to the neutron star mass,  $M$ . (In the models that we consider,  $\delta m/M \lesssim 10^{-11}$  and  $\delta r/R \lesssim 10^{-3}$ .) (3) When approximation (2) is valid, the gravitational redshift correction factor (see Thorne 1977) is given by

$$e^\Phi \equiv 1+z \approx 1+z_s \\ = \left(1 - \frac{2GM}{Rc^2}\right)^{-1/2}, \quad (3)$$

where  $G$  is the universal gravitational constant and  $c$  is the speed of light. Hence, the luminosity gradient term in the equation of energy conservation may be written as

$$e^{-2\Phi} \frac{d}{dr} (L_{\text{tot}} e^{2\Phi}) \approx \frac{dL_{\text{tot}}}{dr}, \quad (4)$$

unless  $dL_{\text{tot}}/dr$  is itself very small. Here,  $L_{\text{tot}}(r)$  is the total luminosity (radiative, conductive, and convective) as measured by an observer at level  $r$ . (In the surface layers that we consider,  $[L_{\text{tot}}(d\Phi/dr)]/(dL_{\text{tot}}/dr) \lesssim 10^{-3}$  at all times.)

With these approximations, the general relativistic equations of stellar structure and evolution can be written in the form

$$\frac{dm}{dr} = 4\pi\rho r^2, \quad (5)$$

$$\frac{dP}{dm} = -\frac{Gm}{4\pi r^4} (1+z_s)^2, \quad (6)$$

$$\frac{dL_{\text{tot}}}{dm} = (\epsilon_{\text{nuc}} - \epsilon_\nu)(1+z_s) - T \frac{ds}{dt} (1+z_s)^2, \quad (7)$$

$$\frac{dT}{dr} = -\frac{3}{16\pi} \frac{\kappa\rho L_{\text{tot}}(1+z_s)}{acr^2 T^3} \\ \text{(radiative zones)}$$

$$= \left(1 - \frac{1}{\Gamma_2}\right) \frac{T}{P} \frac{dP}{dr} \\ \text{(adiabatic convective zones)}. \quad (8)$$

Here,  $\rho$ ,  $P$ ,  $T$ , and  $s$  are the density, pressure, temperature, and specific entropy, respectively,  $t$  is the Schwarzschild coordinate time,  $\epsilon_{\text{nuc}}$  and  $\epsilon_\nu$  are the nuclear energy generation rate and neutrino loss rate, respectively,  $\kappa$  is the combined radiative and conductive opacity,  $\Gamma_2$  is the adiabatic exponent relating pressure to temperature, and  $a$  is the radiation constant. All parameters are as measured by a local observer. We took convection to be efficient in all convective regions (see Joss 1978), so that equation (8) describes the temperature gradient in all cases that we consider.

If we make the variable transformation

$$m_* = (1 + z_s)m, \quad dm_* = (1 + z_s)dm,$$

$$dr_* = (1 + z_s)dr, \quad dt_* = (1 + z_s)^{-1}dt, \quad (9)$$

then equations (5)–(8) can be rewritten as

$$\frac{dm_*}{dr_*} = 4\pi r^2 \rho, \quad (10)$$

$$\frac{dP}{dm_*} = -\frac{Gm_*}{4\pi r^4} \quad (11)$$

$$\frac{dL_{\text{tot}}}{dm_*} = \epsilon_{\text{nuc}} - \epsilon_\nu - T \frac{ds}{dt_*}, \quad (12)$$

$$\frac{dT}{dr_*} = -\frac{3}{16\pi} \frac{\kappa \rho L_{\text{tot}}}{acr^2 T^3}$$

(radiative zones)

$$= \left(1 - \frac{1}{\Gamma_2}\right) \frac{T}{P} \frac{dP}{dr_*}$$

(adiabatic convective zones). (13)

Here  $dr_*$  and  $dt_*$  are the local proper radial distance and time intervals, respectively, and  $m_*(r)$  is an effective mass that determines the local gravity  $g_* = Gm_*/r^2$  at level  $r$ . (Note that  $m_*$  is neither the gravitational mass nor the rest mass enclosed at level  $r$ ; see Misner, Thorne, and Wheeler 1973.) All other variables represent quantities as measured by an observer on the neutron star surface.

Equations (10)–(13) are formally identical to the Newtonian equations describing the structure and evolution, during an incremental time  $dt_*$ , of a region within a star with incremental mass  $dm_*$  and thickness  $dr_*$  a distance  $r$  from the stellar center, where  $r$  encloses mass  $m_*(r)$ . The only distinction between the Newtonian equations of stellar structure and evolution and equations (10)–(13) is that, in the latter equations,  $r$  is *not* the integral of  $dr_*$  from the stellar center to the level under consideration.

By utilizing the above results, we are able to apply our previously developed Newtonian stellar structure and evolution code (see § II) to calculate the general relativistic evolution of the neutron star surface layers. We simply calculate, with the Newtonian code, the

evolution for time  $\delta t_*$  of surface layers of mass  $\delta m_*$  and thickness  $\delta r_*$ , accreting mass at a rate  $\dot{m}_*$  and surrounding a neutron star core of mass  $M_*$  and radius  $R_* = R$ . ( $R$  is the radius measured by an observer on the neutron star surface and is determined by measuring the stellar surface area  $A$  and using the relation  $A = 4\pi R^2$ . It is also the radius quoted in standard neutron star model calculations.) Using equations (9), we then transform these variables into the corresponding quantities that describe the general relativistic evolution, as measured by a distant observer:

$$\delta t = (1 + z_s) \delta t_*, \quad \delta m = (1 + z_s)^{-1} \delta m_*,$$

$$\dot{m} = (1 + z_s)^{-1} \dot{m}_*, \quad \delta r = (1 + z_s)^{-1} \delta r_*,$$

$$M = (1 + z_s)^{-1} M_*, \quad R = R_*. \quad (14)$$

Also, from considerations of energy conservation in general relativity, (see, e.g., Misner, Thorne, and Wheeler 1973), we find that the rate of liberation of energy by accretion (as measured by an observer on the neutron star surface), which we assume to be entirely radiated away as an accretion-driven component of the neutron star surface luminosity (see Joss 1978; Joss and Li 1980), is given by

$$L_{\text{acc}}^{(0)} = z_s(1 + z_s)\dot{m}c^2 = z_s\dot{m}_*c^2. \quad (15)$$

Here,  $\dot{m}$  is the rate of inflow of rest mass (as defined by Misner, Thorne, and Wheeler 1973) at a distance  $r \gg R$  from the neutron star, as measured by a distant observer; hereafter, we shall simply refer to  $\dot{m}$  as the accretion rate. The surface luminosity and effective temperature measured by a distant observer are given by

$$L = (1 + z_s)^{-2} L^{(0)},$$

$$T_e = (1 + z_s)^{-1} T_e^{(0)}, \quad (16)$$

respectively, where  $L^{(0)}$  and  $T_e^{(0)}$  are the luminosity and effective temperature, respectively, as measured by a local observer.

#### IV. THE NUCLEAR REACTION NETWORK

We have used a simplified nuclear reaction network that is partially illustrated in Figure 1 and summarized in Table 1. In addition to the reactions shown in Figure 1, we included the proton-proton,  $^{12}\text{C} + ^{12}\text{C}$ ,  $^{12}\text{C} + ^{16}\text{O}$ , and  $^{16}\text{O} + ^{16}\text{O}$  reactions. However, these reactions, as well as photodisintegration reactions, were always found to be unimportant under the conditions of interest. The reaction rates were taken from Wagoner, Fowler, and Hoyle (1967), Wagoner (1969), and Fowler, Caughlan,

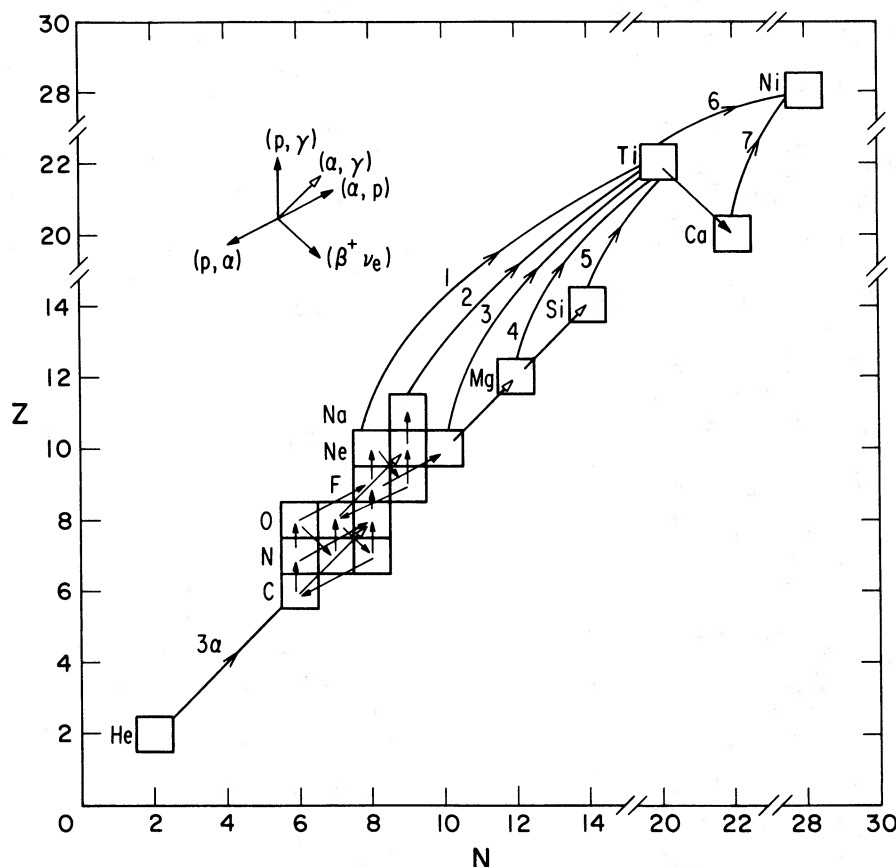


FIG. 1.—The simplified nuclear reaction network employed.  $Z$  and  $N$  are the atomic number and neutron number, respectively, of the 20 nuclear species (including hydrogen, not shown) that comprise the network. Hydrogen burning and helium burning via the rp process was taken into account by use of reaction channels 1 through 7 (see text). Proton-proton,  $^{12}\text{C} + ^{12}\text{C}$ ,  $^{12}\text{C} + ^{16}\text{O}$ ,  $^{16}\text{O} + ^{16}\text{O}$ , and photodisintegration reactions were unimportant under the conditions of interest. The positron decay of  $^{20}\text{Na}$  was neglected, since conditions that allow the production of  $^{20}\text{Na}$  via the reaction  $^{20}\text{Ne}(p, \gamma)^{20}\text{Na}$  will also result in the destruction of this species via  $^{20}\text{Na}(p, \gamma)^{21}\text{Na}$  on a time scale that is short compared to the positron decay time scale.

and Zimmerman (1975). Both weak and strong screening corrections to the reaction rates were taken from Salpeter and Van Horn (1969).

For temperatures less than  $\sim 7 \times 10^7$  K, we adopted the equilibrium CNO reaction rate given by Clayton (1968), while for higher temperatures we used the positron decay-limited “saturated” rate (Hoyle and Fowler 1965; Wallace and Woosley 1981). For  $T \geq 1 \times 10^8$  K, we explicitly calculated the rate of each reaction that contributes appreciably to the cycle. Under conditions for which

$$\frac{dX_{ij}}{dt} \lesssim -\frac{X_i}{\tau}, \quad (17)$$

where  $dX_{ij}/dt$  is the rate of change of the abundance by mass,  $X_i$ , of element  $i$  due to any specific reaction  $j$  and  $\tau$  is the time step used in the numerical evolutionary

calculations, we set  $X_i$  at its equilibrium value, so that

$$\sum_j \frac{dX_{ij}}{dt} = 0. \quad (18)$$

The summation here runs over all reactions that alter the value of  $X_i$ . We reevaluated the equilibrium abundances in each time step, so that such abundances actually continued to vary as other conditions varied in the course of an evolutionary calculation.

As shown by Wallace and Woosley (1981), a breakout from the CNO cycle occurs for  $T \gtrsim 5 \times 10^8$  K, when reaction chains such as  $^{15}\text{O}(\alpha, \gamma)^{19}\text{Ne}(p, \gamma)^{20}\text{Na}$  and  $^{14}\text{O}(\alpha, p)^{17}\text{F}(\alpha, p)^{20}\text{Ne}(p, \gamma)^{21}\text{Na}$  act on intermediate nuclei of the CNO cycle to produce nuclei that are too proton-rich to return to the CNO cycle via positron decays and  $(p, \alpha)$  reactions. Instead, nuclei such as

TABLE 1  
REACTION CHANNELS ADOPTED FOR THE  $rp$  PROCESS<sup>a</sup>

Channel	Reactions Included <sup>b</sup>	Time Scale (s) <sup>c</sup>
1.....	$^{18}\text{Ne} + \left\{ \begin{array}{l} 24(p, \gamma) + 12(\beta^+ \nu_e) \\ 6(p, \gamma) + 6(\alpha, p) \end{array} \right\} \rightarrow ^{42}\text{Ti}$	13.7 $\tau_1$
2.....	$^{20}\text{Na} + \left\{ \begin{array}{l} 22(p, \gamma) + 11(\beta^+ \nu_e) \\ 7(p, \gamma) + (\beta^+ \nu_e) + 5(\alpha, p) \end{array} \right\} \rightarrow ^{42}\text{Ti}$	12.2 $\tau_1$
3.....	$^{20}\text{Ne} + \left\{ \begin{array}{l} 22(p, \gamma) + 12(\beta^+ \nu_e) \\ 7(p, \gamma) + 5(\alpha, p) \end{array} \right\} \rightarrow ^{42}\text{Ti}$	11.9 $\tau_1$
4.....	$^{24}\text{Mg} + \left\{ \begin{array}{l} 18(p, \gamma) + 8(\beta^+ \nu_e) \\ 6(p, \gamma) + 4(\alpha, p) \end{array} \right\} \rightarrow ^{42}\text{Ti}$	9.7 $\tau_1$
5.....	$^{28}\text{Si} + \left\{ \begin{array}{l} 14(p, \gamma) + 6(\beta^+ \nu_e) \\ 5(p, \gamma) + 3(\alpha, p) \end{array} \right\} \rightarrow ^{42}\text{Ti}$	7.3 $\tau_1$
6.....	$^{42}\text{Ti} + \left\{ \begin{array}{l} 14(p, \gamma) + 8(\beta^+ \nu_e) \\ 2(p, \gamma) + 4(\alpha, p) \end{array} \right\} \rightarrow ^{56}\text{Ni}$	7.6 $\tau_2$
7.....	$^{42}\text{Ca} + \left\{ \begin{array}{l} 14(p, \gamma) + 6(\beta^+ \nu_e) \\ 5(p, \gamma) + 3(\alpha, p) \end{array} \right\} \rightarrow ^{56}\text{Ni}$	5.1 $\tau_2$

<sup>a</sup>See text for explanation.

<sup>b</sup>The nuclear species shown are the "seed" (starting) nucleus and the termination point of each channel. The upper and lower lines within curly braces give the number of reactions of each type when positron decays and  $(\alpha, p)$  reactions, respectively, dominate the timescale for a seed nucleus to traverse the channel (see text).

<sup>c</sup>The upper and lower lines give the total time scale for a seed nucleus to traverse the channel when positron decays and  $(\alpha, p)$  reactions, respectively, dominate the time scale. Here  $\tau_1 = \tau_{\alpha p}(^{34}\text{A}) + \tau_{\alpha p}(^{37}\text{K})$  and  $\tau_2 = \tau_{\alpha p}(^{46}\text{Cr}) + \tau_{\alpha p}(^{50}\text{Fe})$  (see text). When positron decays dominate, the total time scale is estimated from the sum of the decay time scales along the appropriate path in the full reaction network (see Wallace and Woosley 1981) from the seed nucleus to the termination point. The individual decay time scales, in turn, are taken from published experimental values (see, e.g., Lederer, Hollander, and Perlman 1967), or estimated from eq. (20) in cases where no experimental information is available.

$^{20}\text{Na}$  and  $^{21}\text{Na}$  undergo a series of proton photcaptures, positron decays, and  $(\alpha, p)$  reactions until they reach the vicinity of the iron-peak nuclei, by which point the relevant reaction rates have become considerably longer. Wallace and Woosley (1981) call this process the  $rp$  (rapid proton) process, although it is capable of consuming both hydrogen and helium.

Our reaction network includes an approximate scheme to take the  $rp$  process into account. This scheme, described below, is based largely on a preliminary version (Woosley and Wallace 1979) of the work by Wallace and Woosley (1981). Our scheme is similar to the simplified reaction network in the APPROX code described by Wallace and Woosley (1981) and incorporates essentially the same physics.

In our scheme, we assume that the  $rp$  process is important when the time scales for proton capture onto the moderately heavy "seed" nuclei that can no longer return to the CNO cycle are less than  $\sim 1$  s. When this criterion is met, the proton-capture time scales are sufficiently short that the  $rp$  process can be a significant means of consuming hydrogen and/or helium on the evolutionary time scales of interest ( $\lesssim 10^2$  s). Moreover,

this criterion ensures that the time scale for synthesis of the seed nuclei into iron-peak elements is dominated by positron decays rather than by the proton captures themselves. In practice, whenever

$$\tau_{p\gamma}(^{20}\text{Ne}) < 1 \text{ s}, \quad (19)$$

where  $\tau_{p\gamma}(^{20}\text{Ne})$  is the time scale for proton photcapture by  $^{20}\text{Ne}$  (taken from Fowler, Caughlan, and Zimmerman 1975), we consider the  $rp$  process to be operative.

We approximate the  $rp$  process by seven reaction channels (see Fig. 1 and Table 1). Channels 1–5 commence on the seed nuclei  $^{18}\text{Ne}$ ,  $^{20}\text{Ne}$ ,  $^{20}\text{Na}$ ,  $^{24}\text{Mg}$ , and  $^{28}\text{Si}$ , respectively, and terminate on  $^{42}\text{Ti}$ . [The  $^{18}\text{Ne}$  nucleus is the only one of these seed nuclei that is capable of being returned to the CNO cycle following a positron decay. However, when the production of  $^{18}\text{Ne}$  by  $^{17}\text{F}(p, \gamma)^{18}\text{Ne}$  is important, this nucleus generally enters the  $rp$  process and only rarely returns to the CNO cycle.] The  $^{42}\text{Ti}$  nucleus is allowed, in turn, to undergo two positron decays to become  $^{42}\text{Ca}$ . Channels 6 and 7 commence on  $^{42}\text{Ti}$  and  $^{42}\text{Ca}$ , respectively, and terminate

on  $^{56}\text{Ni}$ . The seed nuclei themselves are generated by  $\alpha$ -captures and proton captures on nuclei that participate in the CNO cycle; when the  $rp$  process is operative, we continue to calculate in detail the individual reactions of the CNO cycle and the reactions that generate the seed nuclei. The nucleus  $^{56}\text{Ni}$  is chosen as the effective endpoint of the  $rp$  process, since the time scale for further proton captures or  $\alpha$ -captures on  $^{56}\text{Ni}$  is relatively long due to the high Coulomb barrier, and since the positron decay of  $^{56}\text{Ni}$  is highly forbidden and the  $\beta$ -decay time scale is therefore very long (see § VIe below and Wallace and Woosley 1981 for further discussions of these points).

When the  $rp$  process is operative at relatively low temperatures, the only reactions of importance are proton photocaptures (when energetically allowed) and positron decays (by those nuclei which are so proton-rich that further proton captures are forbidden). We assume that the proton capture reactions are much faster than the positron decays, so that the total time scale for each channel in the  $rp$  process is just the sum of the relevant positron decay time scales,  $\tau_\beta$ . Whenever experimental information was available, we simply adopted the measured positron decay rates. These rates should not be appreciably altered by the capture of continuum electrons (see, however, the discussion of  $^{56}\text{Ni}$  decay in § VIe). Experimental data pertaining to the acceleration of such rates by decays from thermally populated excited states are very sparse, but it is likely that most of these rates will not be grossly affected under the relevant conditions.

For several of the proton-rich nuclei, no experimental information on positron decay rates is available. For these nuclei, the following algorithm was used to obtain a guess for the time scale:

$$\begin{aligned} \tau_\beta &\approx 1 \text{ s} && \text{for } w \leq 1 \\ &\approx 1.5 \text{ s} && \text{for } 1 < w \leq 2 \\ &\approx 2 \text{ s} && \text{for } w > 2, \\ w &\equiv 0.2(E/10 \text{ MeV})^{-5}, && (20) \end{aligned}$$

where  $E$  is the total energy released in the decay and  $w^{-1}$  is a rough measure of the phase space available to the decay. For decays involving nuclei whose masses have not been measured experimentally, we estimated the value of  $E$  with the help of a semiempirical mass formula. The total positron decay time scale that we adopted for each channel of the process is listed in Table 1.

We corrected the energy generation rate due to the  $rp$  process for the energy lost to the neutrinos emitted in positron decays. For this purpose, we simply took the average neutrino loss to be 1 MeV per decay.

As the temperature rises, the positron decays in the  $rp$  process are replaced by  $(\alpha, p)$  reactions, so that the process becomes primarily a series of  $(\alpha, p)$  and proton photocapture reactions. With increasing temperature, the  $(\alpha, p)$  reactions become important in successively heavier nuclei with higher Coulomb barriers.

In channels 1–5 of our simplified network, we approximate this trend by comparing the time scale,  $\tau_{\alpha p}(^{30}\text{S})$ , for  $(\alpha, p)$  reactions on the typical intermediate nucleus  $^{30}\text{S}$  with a typical positron-decay time scale ( $\sim 1$  s). [The rate for  $^{30}\text{S}(\alpha, p)^{33}\text{Cl}$ , as well as for all other  $(\alpha, p)$  reactions involved in the  $rp$  process, has not been measured experimentally; we have, instead, derived theoretical estimates for all such rates by use of the methods described by Woosley *et al.* 1975.] If  $\tau_{\alpha p}(^{30}\text{S}) < 1$  s, we assume that the seed nuclei of channels 1–5 are synthesized into  $^{42}\text{Ti}$  by a series of  $(\alpha, p)$  reactions and proton photocaptures, with no positron decays (or, at most, one such decay); otherwise, we assume that  $^{42}\text{Ti}$  is produced by a series of proton photocaptures and positron decays, with no  $(\alpha, p)$  reactions. The number of reactions of each type that are assumed to occur in each channel is given in Table 1. Whenever  $(\alpha, p)$  reactions occur in channels 1–5, the time scale for a seed nucleus to be synthesized into  $^{42}\text{Ti}$  is taken to be the sum of the estimated time scales of  $(\alpha, p)$  reactions on the intermediate nuclei  $^{34}\text{A}$  and  $^{37}\text{K}$ . The nuclei  $^{34}\text{A}$  and  $^{37}\text{K}$  are chosen to represent to two most massive nuclei on which  $(\alpha, p)$  reactions occur in each of these channels; due to the increase in the Coulomb barrier with increasing atomic charge of each reacting nucleus, the time scales of the last two  $(\alpha, p)$  reactions should dominate the time scales of proton photocaptures and of  $(\alpha, p)$  reactions on lighter nuclei in the same channels.

For channels 6 and 7, we treat the increasing importance of  $(\alpha, p)$  reactions with increasing temperature in an analogous manner. When the estimated time scale for  $(\alpha, p)$  reactions on the typical intermediate nucleus  $^{46}\text{Cr}$  is less than 1 s, the synthesis of  $^{56}\text{Ni}$  from  $^{42}\text{Ti}$  and  $^{42}\text{Ca}$  in channels 6 and 7 is considered to consist of a series of  $(\alpha, p)$  reactions and proton photocaptures only; otherwise, the synthesis is taken to consist of proton photocaptures and positron decays only. The number of reactions of each type assumed for both channels and both cases is given in Table 1. The time scale for the synthesis of  $^{56}\text{Ni}$  from  $^{42}\text{Ti}$  and  $^{42}\text{Ca}$  in each channel, when  $(\alpha, p)$  reactions predominate, is taken to be the sum of the estimated time scales for  $(\alpha, p)$  reactions on the intermediate nuclei  $^{46}\text{Cr}$  and  $^{50}\text{Fe}$ , which are chosen to represent the two most massive nuclei on which such reactions occur; the time scales for proton photocaptures and for  $(\alpha, p)$  reactions on lighter nuclei in each channel [all of which have lower Coulomb barriers than  $(\alpha, p)$  reactions on  $^{46}\text{Cr}$  and  $^{50}\text{Fe}$ ] are taken to be negligibly short in comparison.

It is important to realize that the  $rp$  process entails the consumption of both hydrogen and helium. The process takes place on time scales that are generally too long to contribute to the thermal instability that gives rise to neutron star thermonuclear flashes but are sufficiently short to contribute strongly to the energetics of X-ray bursts that result from such flashes. The behavior of the process is significantly modified if hydrogen or helium is largely exhausted while the process is taking place, but our treatment of the process, as described above, automatically includes such modifications.

Our scheme for approximating the  $rp$  process, while considerably simplified, takes into account all of the physics of the process that is important in the context of neutron star thermonuclear flashes. Wallace and Woosley (1981) tested their APPROX code for simulating the  $rp$  process by using it to compute the nuclear energy generation for conditions encountered in models 1 and 5 of neutron star thermonuclear flashes calculated by Taam (1980). We have tested our network by using it to calculate energy generation under similar conditions, and find that it gives results in closer agreement to the full reaction network by Wallace and Woosley (1981) than does APPROX.

## V. RESULTS

We have carried out a series of numerical calculations to study the evolution of the surface layers of accreting neutron stars. Our assumptions and approximations, including our method of incorporating the general relativistic corrections to the equations of stellar structure and evolution and the nuclear reaction network that we employed, are described in the preceding sections. The basic properties of the models and some of the key results that we obtained are summarized in Figure 2 and Table 2. All numerical quantities in Table 2 and in the discussion below are as measured by a distant observer, unless otherwise noted.

### a) The Standard Model

In model 1, which we shall call the standard model, we assumed that the neutron star has a mass of  $M = 1.41 M_{\odot}$ , a radius of  $R = 6.57$  km, a core temperature (as measured by an observer on the neutron star surface) of  $T_c = 1.5 \times 10^8$  K, and no surface magnetic field. (Strictly speaking,  $T_c$  is the temperature at the inner boundary of the neutron star surface layers, which corresponds to a density of  $\sim 10^7$  g cm $^{-3}$  as measured by an observer on the neutron star surface; see § II.) The accretion rate onto the neutron star surface was taken to be  $\dot{m} = 3 \times 10^{16}$  g s $^{-1}$ ; and the abundances, by mass, of hydrogen, helium, and heavy elements in the accreting material were taken to be  $X = 0.69$ ,  $Y = 0.30$ , and  $Z = 0.01$ , respectively. The heavy elements, in turn, were assumed to comprise 50%  $^{12}\text{C}$  and 50%  $^{16}\text{O}$  by mass.

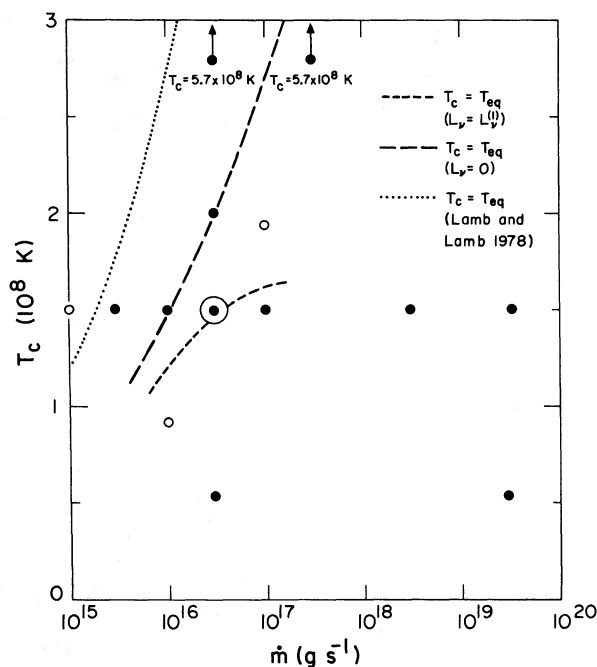


FIG. 2.—The assumed accretion rates,  $\dot{m}$ , and core temperatures,  $T_c$ , employed in the model calculations. The filled circles represent models for which full evolutionary computations were carried out, while the small open circles represent incomplete or less accurate model computations (see text). The large circle surrounding a filled circle denotes the parameter values of the standard model; we have carried out additional evolutionary calculations, wherein other parameters (the neutron star mass, radius, and surface magnetic field strength, as well as the metallicity of the accreting matter) were varied about the values used in the standard model. The light dashed curve is the locus of parameter values for which the core of the neutron star is found to be in thermal equilibrium ( $T_c = T_{\text{eq}}$ ), provided that the neutrino loss rate from the core is given by eq. (1) with  $(1+z_c)/(1+z_s) = 2.12$  (i.e.,  $L_\nu = L_\nu^{(1)}$ ). The heavy dashed curve is the locus of thermal equilibrium conditions when neutrino emission from the core is neglected ( $L_\nu = 0$ ), while the dotted curve represents the equilibrium conditions as originally estimated by Lamb and Lamb (1978) (see text).

Figure 3 shows the variation with time of the surface photon luminosity,  $L$ , and nuclear energy generation rate,  $L_{\text{nuc}}$ , for the first thermonuclear flash in the standard model. (Henceforth, we shall refer to  $L$  simply as the “luminosity.”) Time  $t = 0$  corresponds to the onset of accretion onto the neutron star surface, and the flash commences after a time  $t_R$  of  $\sim 4.7$  hours has elapsed and a total rest mass,  $\Delta M = \dot{m}t_R$ , of  $\sim 5 \times 10^{20}$  g has accreted onto the neutron star. (We shall refer to  $t_R$  as the recurrence time between flashes, but, as will be discussed below, under many circumstances the recurrence intervals between successive flashes may vary.)

At the commencement of the flash, the base of the freshly accreted material has reached a density,  $\rho_{\text{bm}}$ , of  $\sim 9 \times 10^5$  g cm $^{-3}$  (as measured by an observer on the

TABLE 2  
 PROPERTIES OF THE NUMERICAL MODELS<sup>a</sup>

Model Number	$M$ ( $M_{\odot}$ )	$R$ (km)	$T_c$ ( $10^8$ K)	$B$ ( $10^{12}$ gauss)	$\dot{m}$ ( $10^{16}$ g s <sup>-1</sup> )	$L_{\text{acc}}$ ( $10^{38}$ ergs s <sup>-1</sup> )	$Z$
1.....	1.41	6.57	1.5	0.	3.	0.106	0.01
2.....	1.41	6.57	1.5	0.	0.1	0.0035	0.01
3.....	1.41	6.57	1.5	0.	0.3	0.0106	0.01
4.....	1.41	6.57	1.5	0.	1.	0.035	0.01
5.....	1.41	6.57	1.5	0.	10.	0.35	0.01
6.....	1.41	6.57	1.5	0.	300.	10.6 <sup>(f)</sup>	0.01
7.....	1.41	6.57	1.5	0.	3000.	106. <sup>(f)</sup>	0.01
8.....	1.41	6.57	0.54	0.	3.	0.106	0.01
9.....	1.41	6.57	2.0	0.	3.	0.106	0.01
10.....	1.41	6.57	5.74	0.	3.	0.106	0.01
11.....	1.41	6.57	0.54	0.	3000.	106. <sup>(f)</sup>	0.01
12.....	1.41	6.57	5.74	0.	30.	1.06	0.01
13.....	0.705	6.57	1.5	0.	3.	0.106	0.01
14.....	1.41	13.14	1.5	0.	3.	0.106	0.01
15.....	1.41	6.57	1.5	3.	3.	0.106	0.01
16.....	1.41	6.57	1.5	0.	3.	0.106	0.001
17.....	1.41	6.57	1.5	0.	3.	0.106	0.01

Model Number	$X_b^b$	$X_{\text{res}}^b$	$t_R$ (s)	$\tau_r$ (s)	$\tau_d$ (s)	$L_{m1}$ ( $10^{38}$ ergs s <sup>-1</sup> )	$L_{m2}$ ( $10^{38}$ ergs s <sup>-1</sup> )	$T_{\text{em}}$ ( $10^7$ K)	$T_{\text{bm}}$ ( $10^9$ K)
1.....	0.59	0.015	16980	0.7	34	0.49	0.50	1.56	1.48
2.....	$<10^{-8}$	...	$>1.6 \times 10^5$	...	...	...	...	...	...
3.....	0.0004	0.098	58710	4.2	7	0.25	...	1.32	0.95
4.....	0.42	0.018	35410	0.3	16	0.40	0.48	1.56	1.30
5.....	0.66	0.080	6690	0.2	19 <sup>d</sup>	1.20	...	1.94	2.00
6.....	0.65	0.110 <sup>e</sup>	110	11.	21	10.9 <sup>f</sup>	...	3.38	1.23
7.....	...	...	...	...	...	...	...	...	...
8.....	0.66	0.08	31400	0.1	16 <sup>d</sup>	0.98	...	1.85	2.12
9.....	0.63	0.022	15240	0.2	30	0.49	0.50	1.56	1.46
10.....	...	...	...	...	...	...	...	...	...
11.....	...	...	...	...	...	...	...	...	...
12.....	0.45	0.052	590	12.	22	1.25	...	1.96	0.81
13.....	0.56	0.055	15770	22.	31	0.56	...	1.87	1.26
14.....	0.34	0.076	47620	21.	35	1.15	...	1.59	1.04
15.....	0.43	0.20	56590	2.6	34	1.04	...	1.87	2.33
16.....	0.65	0.40	40440	5.8	38	0.75	...	1.73	2.07
17.....	0.52	0.044	11830	11.	16	1.01	...	2.39	1.24

neutron star surface). Up to this time, hydrogen has been burning via the CNO cycle, which is modified somewhat by the high temperatures (up to  $\sim 2 \times 10^8$  K as measured by an observer on the surface) that are achieved in the accreted matter (see § IV). In particular, the noninfinitesimal lifetimes of the  $\beta$ -unstable nuclei (such as  $^{14}\text{O}$  and  $^{15}\text{O}$ ) that participate in the cycle prevent the energy generation rate due to the CNO cycle from surpassing the “saturated” value of

$$\epsilon_{\text{CNO}} \approx 5.86 \times 10^{13} \left( \frac{Z_{\text{CNO}}}{10^{-2}} \right) \text{ ergs g}^{-1} \text{ s}^{-1} \quad (21)$$

(Hoyle and Fowler 1965; Wallace and Woosley 1981), where  $Z_{\text{CNO}}$  is the fractional abundance, by mass, of the moderately heavy elements that participate in the cycle. Consequently, the hydrogen-burning reactions are un-

able to become thermally unstable, except at relatively low temperatures (and then only until the temperature of the burning shell rises to  $\sim 7 \times 10^7$  K, at which point the CNO energy generation rate quickly saturates at  $\epsilon_{\text{CNO}}$ ), so that hydrogen burning generally will not result in significant thermonuclear flashes on accreting neutron stars (Joss 1977; Lamb and Lamb 1978). In model 1, as well as all other models that we have calculated, the thermal instability leading to detectable thermonuclear flashes results directly and exclusively from helium-burning nuclear reactions (although, of course, the presence of hydrogen indirectly alters the strength of the instability by reducing the concentration of helium). After the flash begins, however, the amount of energy that can be released is substantially increased by the presence of hydrogen, which can participate in proton-capture reactions onto the moderately heavy nuclei gen-

TABLE 2—Continued

Model Number	$\rho_{\text{bm}}$ ( $10^6 \text{ g cm}^{-3}$ )	$m_{\text{rad}}$ ( $10^{20} \text{ g}$ )	$\Delta M$ ( $10^{20} \text{ g}$ )	$E_{\text{tot}}$ ( $10^{39} \text{ ergs}$ )	$E_b$ ( $10^{39} \text{ ergs}$ )	$\alpha$	Notes
1.....	0.9	0.28	5.1	1.6	1.3	136	Standard model
2.....	> 0.9	...	> 1.6	> 0.33	...	...	<sup>c</sup>
3.....	0.7	0.10	1.8	0.41	0.16	426	
4.....	0.9	0.10	3.5	1.1	0.68	182	
5.....	1.2	0.06	6.7	2.3	2.1	112	
6.....	0.6	3.0	3.0	0.93	0.60	195	<sup>g</sup>
7.....	...	...	...	...	...	...	No flashes
8.....	1.4	0.05	9.4	2.6	2.2	151	
9.....	0.9	0.18	4.6	1.5	1.2	137	
10.....	...	...	...	...	...	...	No flashes
11.....	...	...	...	...	...	...	No flashes
12.....	0.3	0.17	1.8	0.54	0.38	167	
13.....	0.6	0.25	4.7	2.1	1.2	59	Low mass
14.....	0.4	3.1	14.3	5.9	3.7	59	Large radius
15.....	2.4	0.07	17.0	5.1	3.3	182	High $B$
16.....	1.6	0.06	12.1	4.3	1.5	278	Low $Z$
17.....	0.7	0.17	3.6	1.9	1.4	74	Nonrelativistic

<sup>a</sup> See text for explanation and definitions of symbols.

<sup>b</sup> Note that  $X_b$  is the hydrogen abundance, by mass, at the *base* of the freshly accreted material prior to the flash, while  $X_{\text{res}}$  is the *mass-averaged* residual hydrogen abundance, by mass, within the accreted matter at a time 100 s after the peak of the flash.

<sup>c</sup> The numerical calculations in model 2 were stopped  $\sim 44.6$  hours after the onset of accretion, prior to the development of a thermonuclear flash (see text).

<sup>d</sup> The values of  $\tau_d$  for models 5 and 8 do not reflect the long “tails” on the profiles of these bursts (see text and Figs. 6 and 7).

<sup>e</sup> In model 6 only,  $X_{\text{res}}$  is the residual hydrogen abundance at a time 50 s after the peak of the flash.

<sup>f</sup> The violation of the Eddington limit in models 6, 7, and 11 is an artifact of our treatment of the accretion-driven luminosity (see text).

<sup>g</sup> Flashes subsequent to the first flash are completely suppressed in model 6 (see text), so that the given parameter values refer only to the interval from the onset of accretion to 50 s after the peak of the first flash. The flash is so weak that the nuclear burning shell never becomes convective, so that  $m_{\text{rad}} = \Delta M$ .

erated by helium burning (see § IV). In model 1, the mass fraction of hydrogen declines, due to quiescent burning, from  $X = 0.69$  in the freshly accreted matter to  $X_b = 0.59$  at the base of the accreted envelope when the flash commences. The full evolution of  $L_{\text{nuc}}$  from  $t = 0$  to past the peak of the flash is shown in Figure 4.

Despite the unique role of the triple-alpha reaction during the initial rise in  $L_{\text{nuc}}$ , its contribution to the peak energy generation rate ( $\sim 8 \times 10^{38} \text{ ergs s}^{-1}$ ) is small compared to the contributions of the reactions  $^{14}\text{O}(\alpha, p)^{17}\text{F}$ ,  $^{15}\text{O}(\alpha, \gamma)^{19}\text{Ne}$ , and  $^{17}\text{F}(p, \gamma)^{18}\text{Ne}$ , because of a leveling off of the triple-alpha reaction rate at the prevailing high temperatures ( $\gtrsim 10^9 \text{ K}$ ). The rise time of the luminosity,  $\tau$ , (the time required for  $L$  to increase from a value 10% higher than the steady accretion-driven luminosity,  $L_{\text{acc}}$ , to its first maximum), was  $\sim 0.7 \text{ s}$ . The subsequent decline in  $L_{\text{nuc}}$  and  $L$  is due to the depletion of helium (see Fig. 3) and the nuclei  $^{14}\text{O}$ ,  $^{15}\text{O}$ , and  $^{17}\text{F}$ . A second, relatively broad maximum in both  $L$  and  $L_{\text{nuc}}$  occurs  $\sim 20 \text{ s}$  later and results primarily from the energy released by proton captures (channels 1–7 of the nuclear reaction network shown in Fig. 1; see § IV) onto the moderately heavy nuclei that are

first produced by helium burning. The temperature never becomes sufficiently high to turn on the  $(\alpha, p)$  reactions in channels 1–7. The first maximum in the luminosity,  $L_{m1}$ , and the second maximum,  $L_{m2}$ , are nearly identical in this case ( $\sim 5.0 \times 10^{37} \text{ ergs s}^{-1}$ ).

Figure 5 shows the evolution, near the base of the flashing surface layers in the standard model, of the abundances of helium, hydrogen,  $^{56}\text{Ni}$  (the heaviest nucleus included in our reaction network; see § IV), and the sum of the abundances of the seed nuclei ( $^{18}\text{Ne}$ ,  $^{20}\text{Ne}$ ,  $^{20}\text{Na}$ ,  $^{24}\text{Mg}$ ,  $^{28}\text{Si}$ ,  $^{42}\text{Ti}$ , and  $^{42}\text{Ca}$ , from which commence channels 1–7, respectively) that are important during rapid hydrogen burning. In the same figure we also plot the time variation of the temperature  $T_b$  at the base of the freshly accreted matter (as measured by a local observer). Notice that  $T_b$  stays virtually constant while  $L_{\text{nuc}}$  increases (toward its second maximum; see Fig. 3) with increasing abundances of the seed nuclei. At the same time, from  $\sim 5 \text{ s}$  to  $\sim 20 \text{ s}$  after the first peak of  $L_{\text{nuc}}$ , the surface layers are stable against convection, and the optical depth from the base of the nuclear burning shell to the neutron-star photosphere decreases by  $\sim 14\%$  as hydrogen is depleted by proton-

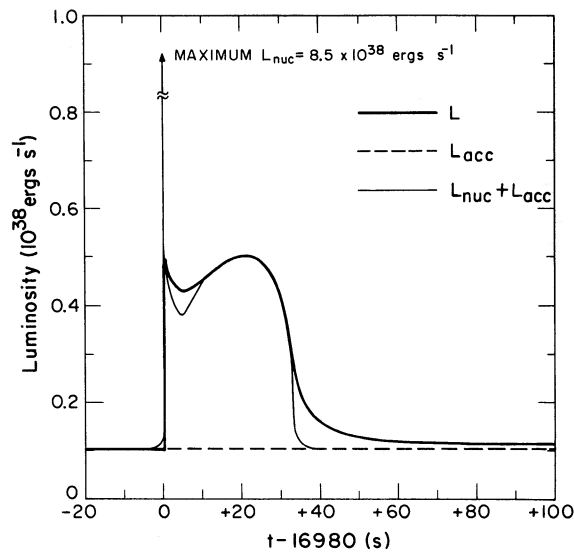


FIG. 3

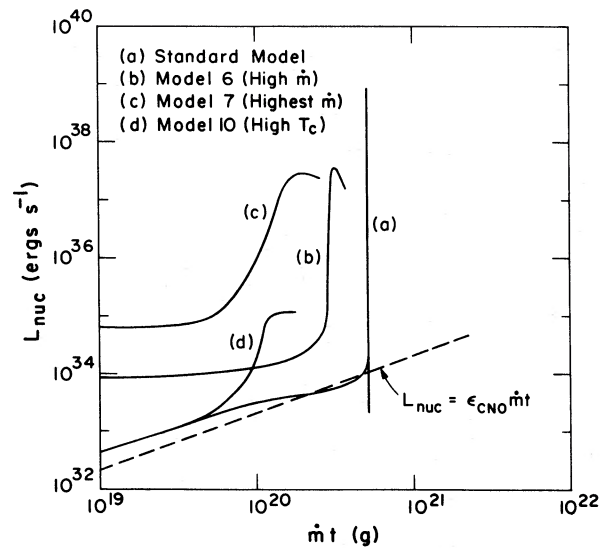


FIG. 4

FIG. 3.—The first X-ray burst following the onset of accretion in the standard model. *Heavy solid curve*, radiated luminosity  $L$  as a function of time during the burst, as measured by a distant observer. Time  $t = 0$  corresponds to the onset of accretion onto the neutron star surface. *Dashed line*, level of persistent accretion-driven luminosity,  $L_{\text{acc}}$ . *Light solid curve*, sum of  $L_{\text{acc}}$  and the nuclear energy generation rate,  $L_{\text{nuc}}$ , as a function of time during the burst. The initial, very sharp peak in  $L_{\text{nuc}}$  represents the thermonuclear flash, which results from helium-burning reactions, while the second, broad maximum results from the consumption of hydrogen via the  $rp$  process (see text).

FIG. 4.—Evolution of the nuclear energy generation rate,  $L_{\text{nuc}}$ , in four models. The quantity  $mt$  represents the total rest mass of the accreted matter at time  $t$  after the onset of accretion onto the neutron star. The dashed line represents the energy generation rate that would result solely from hydrogen burning via the saturated CNO cycle (see eq. [21]) throughout the freshly accreted matter, under the assumption that the fractional abundance of nuclear species in the accreting material that participate in the cycle retains its initial value ( $10^{-2}$  by mass). The relatively strong thermonuclear flash resulting from helium-burning reactions in the standard model (model 1) can be easily distinguished from the relatively weak flash in model 6 and the gradual ignition of helium, with no flash, in each of models 7 and 10.

capture reactions. As a result the surface luminosity increases slowly with increasing  $L_{\text{nuc}}$ , even though  $T_b$  does not vary appreciably.

Due to the large gravitational potential, the surface layers of the neutron star expand very little during the flash. The photospheric radius increases by only  $\sim 10 m$  during the flash, and the emitted radiation should approximate blackbody radiation (Joss 1977). By assuming that the photosphere radiates like a blackbody, we find a maximum effective temperature,  $T_{\text{em}}$ , of the emitted radiation of  $\sim 1.6 \times 10^7$  K. This maximum is achieved during the second maximum in the luminosity, but the maximum effective temperature during the first luminosity peak is very nearly as high. The expansion and subsequent contraction of the surface layers during the flash is highly subsonic, and we do not detect any evidence for dynamical effects in any of our models. However, since our code employs the assumption of hydrostatic equilibrium, we cannot rule out the possibility that dynamical phenomena will develop (Rakavy, Shaviv, and Zinamon 1966, 1967; see § VII for a further discussion).

During the flash and subsequent hydrogen burning, the densities within the surface layers decline because of the expansion, while the temperature at the base of the

freshly accreted material reaches a maximum value,  $T_{\text{bm}}$ , of  $\sim 1.5 \times 10^9$  K (as measured by an observer on the neutron star surface). The convection zone briefly extends outward to include most of the mass of the surface layers; the minimum mass,  $m_{\text{rad}}$ , of the outermost radiative layer when the convection zone has reached its maximal extent is only  $\sim 3 \times 10^{19}$  g. However, at this time the density at base of the radiative zone is still quite high ( $\sim 10^5$  g cm $^{-3}$ ). After reaching its maximal extent, the convection zone shrinks rapidly and disappears entirely  $\sim 0.2$  s after the commencement of the flash. The  $\beta$ -unstable species synthesized by the CNO cycle and the  $rp$  process are mixed throughout the convection zone, but the energy released by the radioactivity of these species does not appreciably increase the spatial or temporal extent of the convection (cf. Taam 1981a). It is highly unlikely that convection will penetrate to the photosphere in any physically realizable situations (Joss 1977, 1978), even when such radioactivity is present.

After passing through the second maximum described above, the luminosity starts to decline as hydrogen is depleted. The total duration of the burst,  $\tau_d$  (the interval between the peak nuclear energy generation by the flash and the time when the luminosity drops to  $1/e$  of its

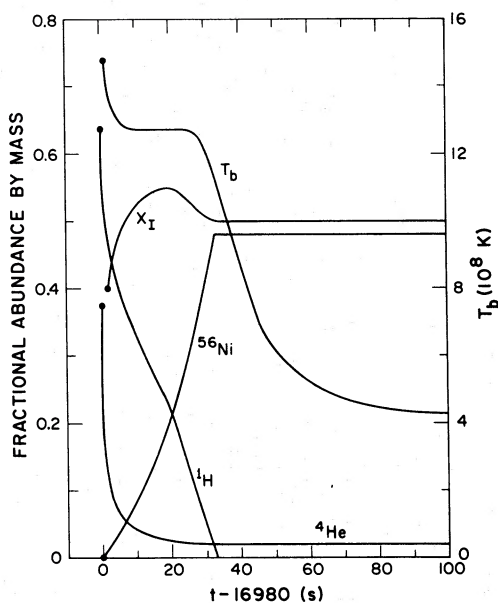


FIG. 5.—Evolution of chemical abundances (*left-hand scale*) and of temperature,  $T_b$  (*right-hand scale*), at the base of the freshly accreted matter during the first thermonuclear flash in the standard model. Time  $t = 0$  corresponds to the onset of accretion onto the neutron star.  $X_I$  is the sum of the fractional abundances, by mass, of the seed nuclei  $^{18}\text{Ne}$ ,  $^{20}\text{Ne}$ ,  $^{20}\text{Na}$ ,  $^{24}\text{Mg}$ ,  $^{28}\text{Si}$ ,  $^{42}\text{Ti}$ , and  $^{42}\text{Ca}$ , from which commence channels 1–7, respectively, of the  $rp$  process (see text).

highest value), is  $\sim 30$  s. The total amount of nuclear energy,  $E_{\text{tot}}$ , available to the flash and the subsequent nuclear burning is  $\sim 1.6 \times 10^{39}$  ergs. Of this,  $E_b \approx 1.3 \times 10^{39}$  ergs is emitted as electromagnetic radiation from the neutron star surface, constituting an observable X-ray burst. Nearly all of the remainder ( $\sim 20\%$  of the total available energy) is either transferred as heat to the core of the neutron star (see §§ II and VI*a*) or gradually emitted from the photosphere on time scales in excess of 100 s. The mass-averaged residual abundances of hydrogen and helium 100 s after the start of the flash are  $X_{\text{res}} \approx 0.015$  and  $Y_{\text{res}} \approx 0.02$ , respectively, so that the flash consumes nearly all of the available nuclear fuel.

The accretion onto the neutron star surface produces a steady accretion-driven luminosity of  $\sim 1 \times 10^{37}$  ergs  $\text{s}^{-1}$ . The ratio,  $\alpha$ , of the time-averaged burst luminosity (emitted up to 100 s after the start of the flash) to accretion-driven luminosity is  $\sim 140$ . This is a factor of  $\sim 2$ – $3$  smaller than the values of  $\alpha$  for pure helium flashes in similar neutron star models (Joss 1978), due to the larger energy content of the hydrogen-rich fuel.

We have carried out a preliminary calculation that follows the evolution of the standard model through a second thermonuclear flash. The second flash commences after only  $\sim 2.2$  hours elapsed since the first flash, and, since a smaller amount of nuclear fuel has accumulated, the second flash is considerably weaker

than the first. We shall present the reasons for this result in § VI*d* (see also § VI*e*); for now, we simply note that evidently the intervals between successive flashes in a given model are not necessarily uniform. We are currently refining and extending our calculations of successive flashes, and we shall present our results elsewhere.

#### b) Variations in Accretion Rate

We have calculated the evolution of the surface layers of a series of accreting neutron star models, in which we systematically varied the parameters of the model relative to those of the standard model. The results of these calculations are summarized in this subsection and the following two subsections.

In models 2–7, we varied  $\dot{m}$  about the value used in the standard model while holding all other parameters fixed. The value of  $\dot{m}$  is successively larger in models 2–4, the standard model, and models 5–7. The X-ray bursts (variation of luminosity with time) from the first resultant thermonuclear flash in each of several of these models are shown in Figure 6.

We calculated the evolution of model 2 ( $\dot{m} = 1 \times 10^{15}$  g  $\text{s}^{-1}$ ) until  $\sim 1.4 \times 10^5$  s after the onset of accretion, when a helium layer began to develop beneath an outer hydrogen-burning shell. The accretion rate here is so low that hydrogen burning via the “saturated” CNO cycle is sufficient to allow the complete consumption of hydrogen before helium ignites in the hydrogen-rich layer (see § VI*d* for a further discussion). Due to the low accretion rate, the mass of the steady hydrogen-burning shell was only  $\sim 6 \times 10^{19}$  g, and the base of this layer maintained a temperature of only  $\sim 1.2 \times 10^8$  K. At this temperature the helium burning was still quite slow ( $\sim 8 \times 10^{11}$  ergs  $\text{g}^{-1} \text{s}^{-1}$ ). To avoid excessive use of computer time, we terminated the calculations before helium ignition, but we expect that helium would ignite in a flash after the development of a rather massive ( $\gtrsim 10^{22}$  g) helium layer beneath the hydrogen-burning shell. We expect that for still lower accretion rates, the steady hydrogen-burning shell will become even thinner and the preflash temperatures even lower. Hence, a deeper helium shell should accumulate as the accretion rate is further reduced, and the resultant flashes should be stronger (at least until pycnonuclear reactions at the base of the helium shell become important) and considerably more widely separated in time (see also Joss 1979; Wallace, Woosley, and Weaver 1981).

In model 3 ( $\dot{m} = 3 \times 10^{15}$  g  $\text{s}^{-1}$ ), a helium layer again developed beneath the hydrogen-burning shell before the helium ignited. Due to the higher accretion rate, the heating of the surface layers by quiescent hydrogen burning was more rapid than in model 2. As a result, the flash commences after only  $\sim 16$  hours have elapsed, at which time only  $\sim 1.8 \times 10^{20}$  g of material have accumulated, and most of this matter is still in the form of unburned hydrogen. The density at the base of the

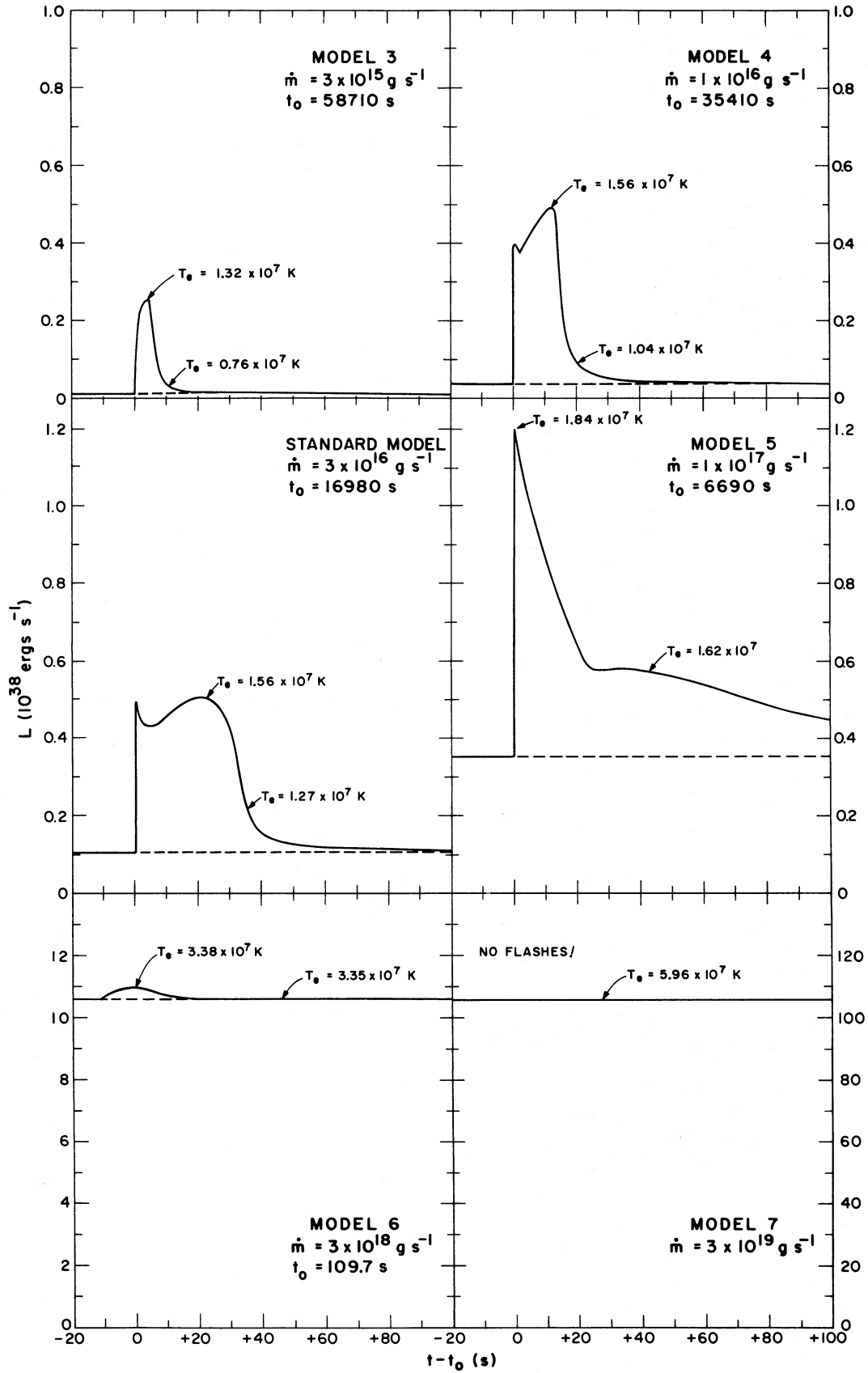


FIG. 6

helium shell is only  $\sim 6 \times 10^5 \text{ g cm}^{-3}$ . The flash is consequently quite weak, with a peak shell temperature ( $T_{\text{bm}} \approx 9.5 \times 10^8 \text{ K}$ ), a peak luminosity ( $L_{m1} \approx 2.5 \times 10^{37} \text{ ergs s}^{-1}$ ), and an emitted burst energy ( $E_b \approx 1.6 \times 10^{38} \text{ ergs}$ ) all substantially smaller than in the standard model. Moreover, although there are still two distinct maxima in  $L_{\text{nuc}}$ , there is only one peak in  $L$  corresponding to the second broad peak in  $L_{\text{nuc}}$ , which results from the  $rp$  process. (We found that, in general, an initial sharp peak in  $L$  is produced only in strong flashes wherein the base temperatures and densities are high; this peak becomes less pronounced as the strength of the flash decreases and disappears entirely when the flash becomes sufficiently weak.) Due to the relatively low accretion rate, the steady consumption of hydrogen depletes the available nuclear energy per unit mass of accreted matter significantly and thereby leads to a large  $\alpha$ -value ( $\alpha \approx 430$ ).

As will be shown in § VI*d*, the accretion rate in model 3 is approximately equal to the critical value at which the hydrogen and helium layers marginally separate prior to a thermonuclear flash. Thus, as  $\dot{m}$  varies, the energy released in the flash passes through a minimum when  $\dot{m} \approx 3 \times 10^{15} \text{ g s}^{-1}$  and the hydrogen and helium shells just separate.

When the accretion rate is increased to  $1 \times 10^{16} \text{ g s}^{-1}$  (model 4), the flash commences after only  $\sim 9.8$  hours have elapsed. As a result, hydrogen burning is not yet completed at the base of the freshly accreted matter when helium ignites, and hydrogen is a major constituent ( $\sim 40\%$  by mass) of the helium-flashing matter at the start of the flash. The flash is fairly strong, due to the high base density ( $\rho_b \approx 9 \times 10^5 \text{ g cm}^{-3}$ ) and initially high helium abundance ( $\sim 48\%$  by mass) compared to that of the standard model. The resultant X-ray burst therefore qualitatively resembles that of the standard model, with a double-peaked structure, luminosity maxima that are comparable to those of the standard model ( $L_{m1} \approx 4.0 \times 10^{37} \text{ ergs s}^{-1}$  and  $L_{m2} \approx 4.8 \times 10^{37} \text{ ergs s}^{-1}$ ), but a smaller amount of emitted burst energy ( $E_b \approx 6.8 \times 10^{38} \text{ ergs}$ ) due to the smaller quantity of accreted matter ( $\Delta M \approx 3.5 \times 10^{20} \text{ g}$ ) that accumulates before the flash commences. The  $\alpha$ -value for this model ( $\sim 180$ ) is intermediate between those of model 3 and the standard model, since the fraction of the hydrogen consumed by steady burning before the flash is neither as small as in the standard model nor as large as in model 3.

Model 5 assumes a higher accretion rate ( $\dot{m} = 1 \times 10^{17} \text{ g s}^{-1}$ ) than that of the standard model. A large quantity

of accreted matter ( $\Delta M \approx 7 \times 10^{20} \text{ g}$ ) accumulates to a high density ( $\rho_{\text{bm}} \approx 1.2 \times 10^6 \text{ g s}^{-1}$ ) before helium ignites (at  $t_R \approx 1.9$  hours). A strong flash results, with a fast rise ( $\tau_r \approx 0.2 \text{ s}$ ), a high peak burst luminosity ( $L_{m1} \approx 1.2 \times 10^{38} \text{ ergs s}^{-1}$ ), and a high total burst emission ( $E_b \approx 2.1 \times 10^{39} \text{ ergs}$ ). The peak shell-burning temperature is so high ( $T_{\text{bm}} \approx 2.0 \times 10^9 \text{ K}$ ) that ( $\alpha, p$ ) reactions become important in the  $rp$  process (see § IV). As a result, the consumption of hydrogen by proton-capture reactions in the  $rp$  process is greatly retarded; there is no secondary peak in the burst luminosity, but rather a plateau at a luminosity of  $\sim 6 \times 10^{37} \text{ ergs s}^{-1}$  followed by a slow decline lasting for at least 100 s.

The calculation of model 5 was terminated  $\sim 100$  s after the start of the flash, in order to avoid an excessive use of computer time. The  $\alpha$ -value for this model given in Table 2 ( $\alpha \approx 110$ ), as well as for all other models, is based on the burst emission during only the first 100 s after the flash, and does not take into account any emission in a burst "tail" at later times after the flash.

When the accretion rate is increased another factor of  $\sim 30$ , to  $\dot{m} \approx 3 \times 10^{18} \text{ g s}^{-1}$  (model 6), the behavior of the model is radically different. Heating due to gravitational compression of the accreting material is dominant over heating due to hydrogen burning (see § VI*d*). Hence, the helium ignites after only 1.8 minutes have elapsed; the base density is only  $\sim 6 \times 10^5 \text{ g cm}^{-3}$  at the start of the flash, and electron degeneracy is always relatively weak throughout the freshly accreted matter due to the effects of compressional heating. As a result, neither  $L_{\text{nuc}}$  nor  $L$  displays a sharp initial peak. Instead,  $L_{\text{nuc}}$  increases smoothly to the rate dictated by the  $rp$ -process rate (see § IV and Fig. 4). The resultant X-ray burst is very inconspicuous;  $L$  has one broad peak which is only  $\sim 3\%$  higher than the persistent accretion-driven luminosity. Following this initial flash the nuclear burning rate achieves a steady state with no subsequent flashes, due to the high temperatures ( $\sim 9 \times 10^8 \text{ K}$ ) maintained at the base of the burning matter and the concomitantly weak temperature dependence of the helium-burning reactions (see § VI*d* for a further discussion). (The strong temperature dependence of the nuclear = reaction rates is a central ingredient of the thin-shell instability that leads to thermal flashes; see Schwarzschild and Härm 1965; Giannone and Weigert 1967; Sugimoto and Fujimoto 1978; Fujimoto, Hanawa, and Miyaji 1981.) When the accretion rate is increased by another factor of 10 to  $\dot{m} = 3 \times 10^{19} \text{ g s}^{-1}$  (model 7), the shell-burning temperatures become so high that the flashes are entirely suppressed, and the accreted surface

FIG. 6.—X-ray burst (radiated luminosity  $L$  as a function of time  $t$ ) resulting from the first thermonuclear flash in the standard model and each of five additional models. All models have the same parameter values as those of the standard model except for the accretion rate,  $\dot{m}$ . In each case the flash starts near  $t = t_0$  (where  $t = 0$  corresponds to the onset of accretion onto the neutron star), the dashed line indicates the levels of persistent accretion-driven luminosity, and the effective temperature,  $T_e$ , is indicated at a few representative points. The systematic trends in the strength and shape of the emitted burst with variations in  $\dot{m}$  (see text) are evident in this figure.

layers rapidly relax toward a state of steady nuclear burning (see Fig. 4). At the very high accretion rates of models 6 and 7 (as well as model 11, which will be discussed in the following subsection), the accretion-driven luminosity exceeds the Eddington limit. However, this formal violation of the Eddington limit has no dynamical consequences, since we neglect any interaction between the accretion-driven luminosity and the accreting matter (Joss 1978). These models are most relevant to discussions of nonspherical accretion onto magnetized neutron stars (see § VI f below), to which the Eddington limit is not directly applicable.

### c) Variations in Core Temperature

In models 8, 9, and 10, the core temperature is varied about that of the standard model ( $T_c = 1.5 \times 10^8$  K), while all other parameters are held fixed. The X-ray bursts resulting from thermonuclear flashes in these models are shown in Figure 7.

Model 8 assumes a core temperature of only  $5.4 \times 10^7$  K. In this case, the heat outflow from the core is relatively unimportant in determining the thermal structure of the freshly accreted surface layers; nuclear burning within the surface layers is by far the most important heat source in this regard. Hydrogen initially ignites in a small flash, due to the temperature sensitivity of the CNO hydrogen-burning rates at the relatively low temperatures within the surface layers, but the hydrogen-burning runaway terminates at a temperature of  $\sim 7 \times 10^7$  K when the energy generation rate saturates at the value given by equation (21). The amount of energy that can be released in such a flash is capable of raising the temperature by no more than  $\sim 1 \times 10^8$  ( $Z_{\text{CNO}}/10^{-2}$ ) K, which is insufficient to lead immediately to a helium flash, and the small hydrogen flash that we obtain should have no observable consequences. However, following the hydrogen flash, the temperature at the base of the freshly accreted matter continues to rise steadily and fairly rapidly, resulting in helium ignition after an additional  $\sim 1 \times 10^3$  s have elapsed. This confirms a scenario envisaged by Fujimoto, Hanawa, and Miyaji (1981), wherein a neutron-star hydrogen flash develops into a helium flash.

A rather thick layer has accumulated ( $\Delta M \approx 9 \times 10^{20}$  g) by the time that helium ignites, at which point the density at the base of the freshly accreted matter has reached  $\sim 1.4 \times 10^6$  g cm $^{-3}$ . As a result, the helium flash is quite strong and closely resembles that of model 5 (aside from the longer time,  $t_R \approx 8.7$  hours, required for the flash to commence at the lower accretion rate of model 8).

In model 9, the core temperature ( $T_c = 2 \times 10^8$  K) is higher than in the standard model, so that the heat flow out of the core plays a slightly larger role in determining the thermal structure of the surface layers than in the standard model. However, the heat released by quies-

cent hydrogen burning is still the most important factor in determining the thermal structure of the burning layers prior to the flash. Consequently, the flash and resultant X-ray burst are very similar to those of the standard model. The flash occurred slightly sooner ( $t_R \approx 4.2$  hours) than in the standard model and resulted in a double-peaked burst with a slightly shorter duration ( $\tau_d \approx 30$  s) and a slightly smaller total burst emission ( $E_b \approx 1.2 \times 10^{39}$  ergs) but nearly identical maximum luminosities. The  $\alpha$ -value was also virtually identical to that of the standard model.

When the core temperature is increased to  $5.74 \times 10^8$  K (model 10), the heat flow out of the core dominates the thermal structure of the surface layers prior to the flash. As a result, the helium ignites when only a small amount of material has accumulated. Due to the high temperatures in the freshly accreted matter and the moderately low accretion rate, the nuclear burning rate becomes sufficiently high to consume the fuel as fast as it is accreted, without the development of a thermal instability. Hence, a state of steady nuclear burning is achieved (see Fig. 4).

Model 11 has the same core temperature as model 9 but a much higher accretion rate ( $T_c = 5.4 \times 10^7$  K and  $\dot{m} = 3 \times 10^{19}$  g s $^{-1}$ ). Because of the high accretion rate, compressional heating is the dominant factor in determining the thermal structure of the surface layers. Consequently, in contrast to the strong flash of model 9, the flash is suppressed in model 11, and  $L_{\text{nuc}}$  simply increases smoothly to its steady value. The evolution of this model is virtually identical to that of model 7, which has the same accretion rate but a higher core temperature.

In model 12, the core temperature is equal to that of model 10 ( $T_c = 5.74 \times 10^8$  K), but the accretion rate is one order of magnitude higher ( $\dot{m} = 3 \times 10^{17}$  g s $^{-1}$ ). In contrast to model 10, the accretion rate is sufficiently high to allow some accumulation of nuclear fuel, despite the high temperatures in the freshly accreted matter. As a result, a rather inconspicuous flash commences at  $t \approx 10$  minutes. As in models 6, 7, and 11, electron degeneracy is relatively unimportant even before the flash commences, and hence the flash is weak, with only one broad peak in  $L$  that is only 20% higher than the steady accretion-driven luminosity. We did not determine whether there would be any subsequent flashes or whether, instead, the surface layers would then relax to a state of steady nuclear burning.

### d) Variations in Neutron Star Mass, Radius, Surface Magnetic Field Strength, and Metallicity of the Accreting Matter

We have calculated the evolution of a series of models (models 13–16) in which the accretion rate and core temperature were held fixed at the values of the standard model but the mass, radius, and surface magnetic

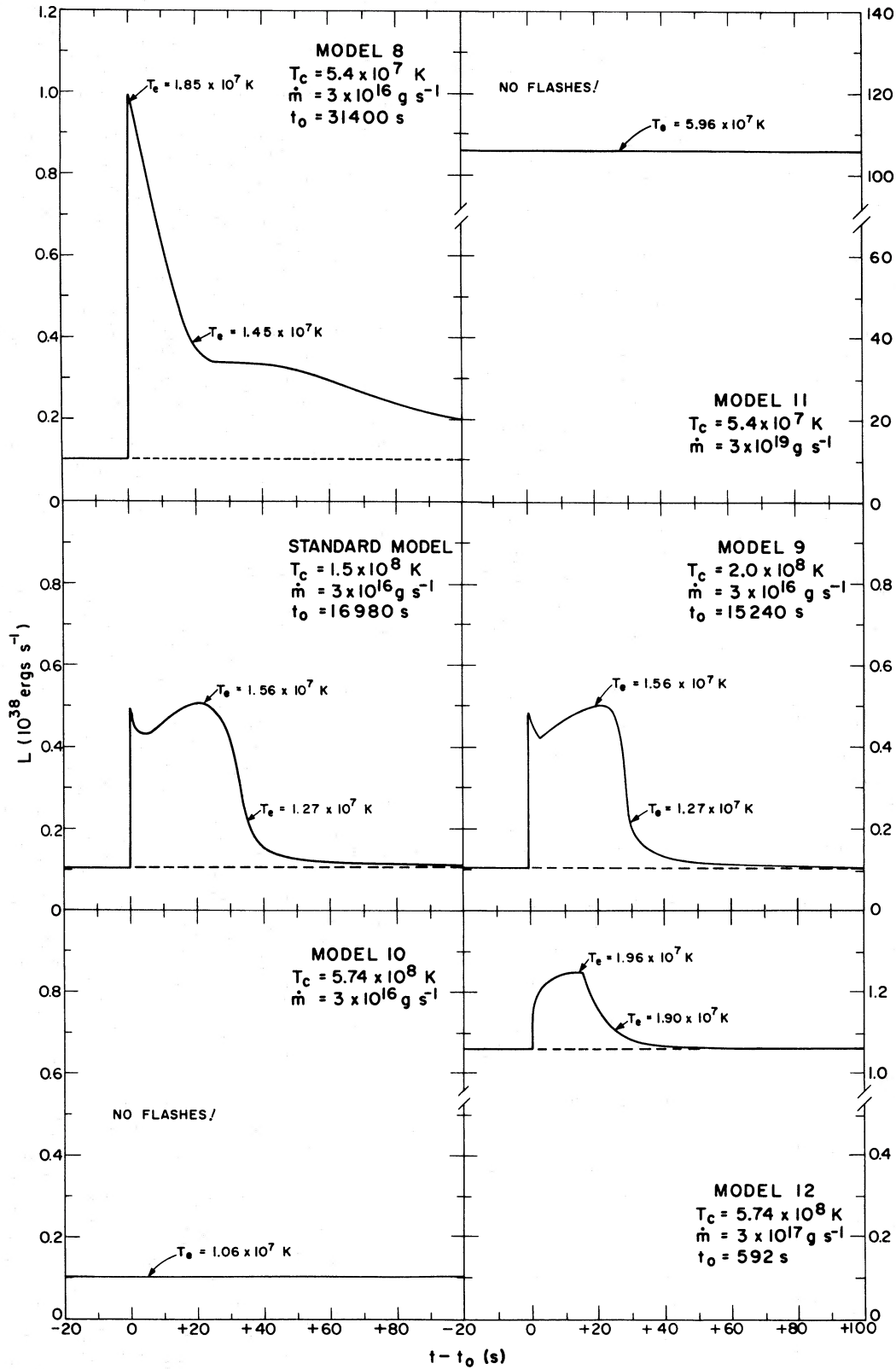


FIG. 7.—Same as Fig. 6, for the standard model and three additional models (models 8, 9, and 10) with the same parameter values as those of the standard model except for the core temperature,  $T_c$ . Also shown are two models, models 11 and 12, which have the same parameter values as those of models 8 and 10, respectively, except for higher accretion rates. The systematic trends in the strength and shape of the emitted burst with variations in  $T_c$ , and with variations in  $\dot{m}$  at very low and very high values of  $T_c$ , are evident in this figure (see text).

field strength of the neutron star and the initial metallicity of the accreting matter were systematically varied about the values of the standard model. The X-ray bursts resulting from thermonuclear flashes in these models are shown in Figure 8.

In model 13, the neutron star mass ( $M = 0.705 M_{\odot}$ ) was taken to be half that of the standard model. The resultant flash, however, is not greatly different from that of the standard model. The elapsed time until helium ignition is slightly shorter ( $t_R \approx 4.4$  hours), and the total burst emission is slightly smaller ( $E_b \approx 1.2 \times 10^{39}$  ergs). The peak burst luminosity ( $L_{m1} \approx 5.6 \times 10^{37}$  ergs  $s^{-1}$ ) is slightly higher, due to the smaller gravitational redshift at the neutron star surface. The peak temperature at the base of the accreted matter ( $T_{bm} \approx 1.3 \times 10^9$  K) is lower than in the standard model, since the pressure at the base is lower when helium ignites. Hence the peak nuclear luminosity is lower, and the surface luminosity has only one relatively broad peak (see § Vb above). The  $\alpha$ -value is a factor of  $\sim 2$  smaller ( $\alpha \approx 60$ ), mainly due to the smaller gravitational potential at the neutron star surface and the concomitantly lower level of steady accretion-driven luminosity.

In model 14, the neutron star radius ( $R = 13.14$  km) was taken to be twice as large as that of the standard model. The effects of increasing the radius were more pronounced than those of decreasing the mass. The time required for the flash to commence ( $t_R \approx 13$  hours) is considerably longer than in the standard model, due largely to the increased neutron star surface area over which the accreted material is spread. The accumulated mass ( $\Delta M \approx 1.4 \times 10^{21}$  g) and the emitted burst energy ( $E_b \approx 3.7 \times 10^{39}$  ergs) are also larger, due to the longer elapsed time until the start of the flash and, in the case of  $E_b$ , to the reduced gravitational redshift from the neutron star surface. Because of the lower surface gravitational potential, the  $\alpha$ -value is reduced to  $\sim 60$ , as in model 13. Also similarly to model 13, the pressure at the base of the accreted matter is reduced relative to that in the standard model, despite the considerably larger value of  $\Delta M$ , so that the luminosity maxima associated with the helium flash and subsequent rapid hydrogen burning are again blended into a single, relatively broad peak. The peak luminosity is much higher ( $L_{max} \approx 1.2 \times 10^{38}$  ergs  $s^{-1}$ ) than in the standard model, simply due to the lower surface gravitational redshift. However, the peak effective temperature is still  $\sim 1.6 \times 10^7$  K, nearly identical to that of the standard model, because of the larger neutron star surface area.

In model 15, the neutron star was taken to have a strong surface magnetic field. The magnetic field strength ( $B = 3 \times 10^{12}$  gauss) was assumed to be uniform across the neutron star surface, and the field was taken to be everywhere perpendicular to the surface. Of course, this idealized situation cannot be realized in practice, but it may adequately approximate the conditions in the mag-

netic polar caps of a magnetized neutron star, wherein the accretion flow is funneled onto the caps. If this is the case, the results for this model, which entails the assumption of spherical symmetry, must be appropriately scaled to take into account the funneling of the accretion flow (Joss and Li 1980; see also § VI f below). We included the reduction in the radiative and conductive opacities resulting from the strong magnetic field, according to the prescription given by Joss and Li (1980), but neglected other effects that such a field might produce. We found that in practice, only the reduction in conductive opacity was quantitatively important.

Due to the suppression of opacities and the resultant increase in the efficiency of heat transport away from the base of the freshly accreted matter, the surface layers remain relatively cool and the helium flash is delayed until  $t_R \approx 16$  hours. By this time, a comparatively large amount of material has accumulated ( $\Delta M \approx 1.7 \times 10^{21}$  g), and the density at the base of the accreted matter is quite high ( $\rho_{bm} \approx 2.4 \times 10^6$  g  $cm^{-3}$ ). The resulting flash is very strong, with a peak shell-burning temperature of  $2.3 \times 10^9$  K. This is sufficiently high to cause ( $\alpha, p$ ) reactions to play a large role in the  $rp$  process (see § IV), so that rapid hydrogen burning by proton-capture reactions in the  $rp$  process is partially suppressed. The emitted burst luminosity therefore exhibits only the first peak due to the helium flash and a relatively slow decline (rather than a secondary maximum) as the hydrogen is relatively gradually consumed. Due to the large amount of energy released, the peak luminosity of the burst ( $L_{m1} \approx 1.0 \times 10^{38}$  ergs  $s^{-1}$ ) is considerably higher than in the standard model. The  $\alpha$ -value ( $\alpha \approx 180$ ) is also higher than in the standard model, due to the rather large fractional amount of hydrogen ( $X_{res} \approx 0.20$ ) that is left unburned after the flash.

In model 16, the initial abundance of heavy elements in the accreting matter was reduced to  $Z = 10^{-3}$  (again taken to be 50%  $^{12}C$  and 50%  $^{16}O$  by mass). Energy generation via the CNO cycle therefore saturates (see § Va) at a value an order of magnitude smaller than in the standard model. Consequently, the evolution of this model is similar to that of model 15. The helium flash is delayed until  $t_R \approx 11$  hours, at which time the mass of the freshly accreted matter is  $\Delta M \approx 1.2 \times 10^{21}$  g and the density at the base of this matter is  $\rho_{bm} \approx 1.6 \times 10^6$  g  $cm^{-3}$ . As in model 15, the resulting flash is very strong, with a peak shell-burning temperature ( $\sim 2.0 \times 10^9$  K) sufficiently high to again cause ( $\alpha, p$ ) reactions to play a major role in the  $rp$  process. Due to the importance of these reactions in reducing the rate of hydrogen burning during the flash, together with the low hydrogen-burning rate via the saturated CNO cycle prior to the flash, the fractional amount of residual hydrogen ( $X_{res} \approx 0.40$ ) is the largest among any of the models that we have calculated. Because of the large

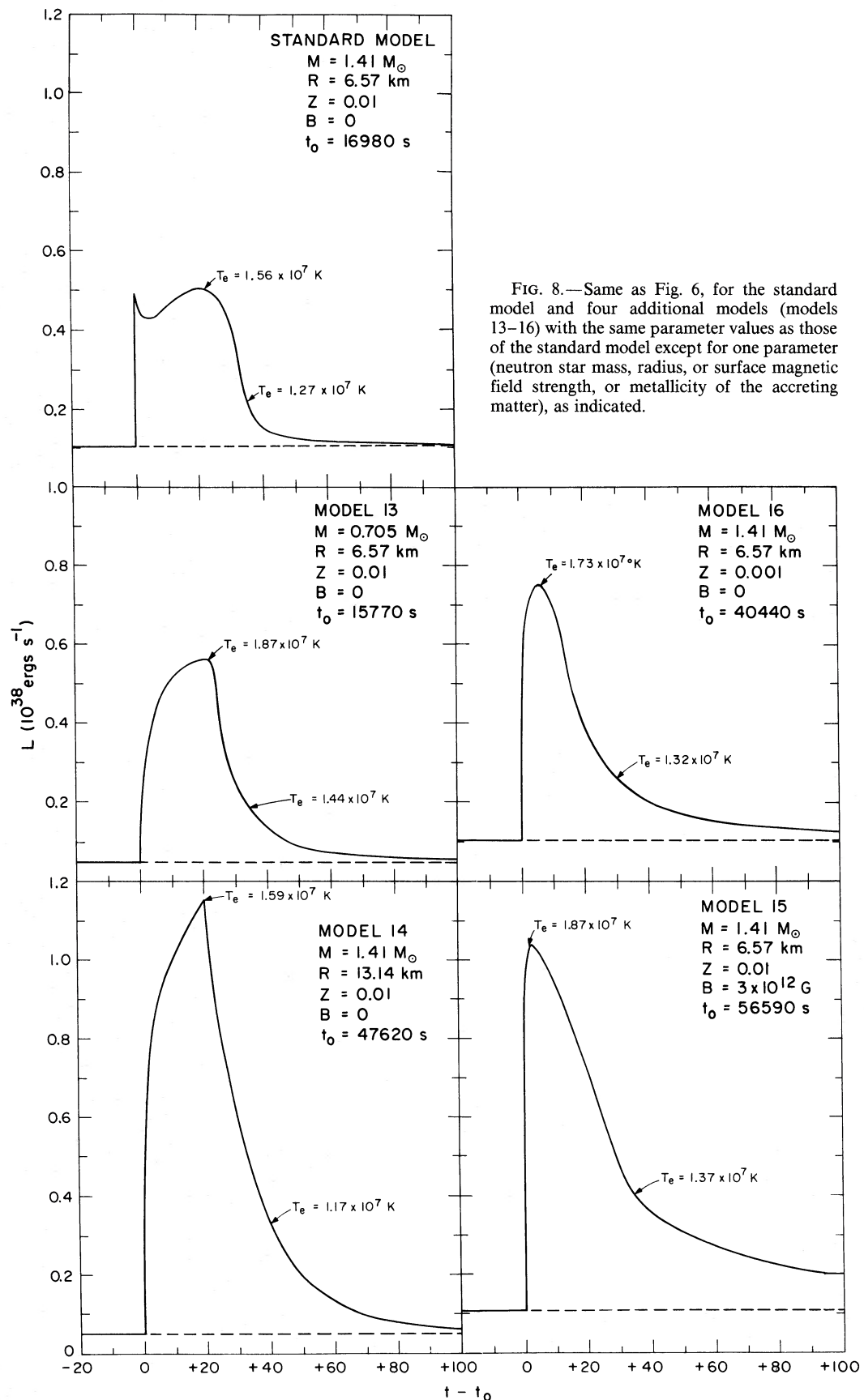


FIG. 8.—Same as Fig. 6, for the standard model and four additional models (models 13–16) with the same parameter values as those of the standard model except for one parameter (neutron star mass, radius, or surface magnetic field strength, or metallicity of the accreting matter), as indicated.

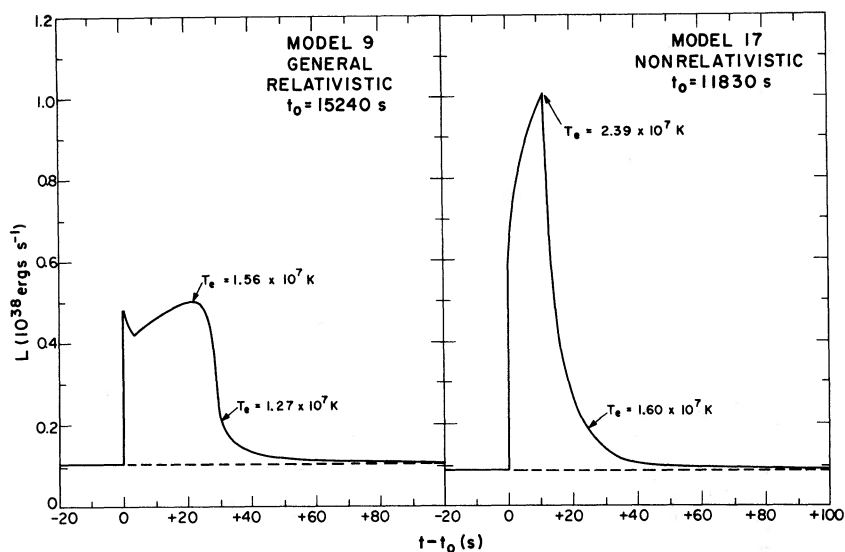


FIG. 9.—Same as Fig. 6 for two models with identical parameter values, but one of which (model 9) is based on a fully general relativistic calculation while the other (model 17) is based on a nonrelativistic calculation. The effects of general relativistic corrections to the equations of stellar structure and evolution on the properties of the emitted bursts are evident from a comparison of these two burst profiles (see text).

amount of unburned fuel, the  $\alpha$ -value is considerably higher than that of the standard model ( $\alpha \approx 280$ ).

#### e) Significance of the General Relativistic Corrections

While some of the consequences of general relativistic effects, notably on the properties of radiation from the neutron star surface, are easy to understand (see the above discussion), the overall impact of the general relativistic corrections upon the structure and evolution of the surface layers is less straightforward. In order to investigate this impact, we calculated the evolution of the surface layers of a neutron star model (model 17) in which we neglected all general relativistic corrections to the equations of stellar structure and evolution (see § III). In order to facilitate a comparison with a general relativistic calculation, the parameters of the model were chosen to be identical to those of model 9 (except that, of course, all parameters in model 17 have Newtonian definitions).

The X-ray burst resulting from the first thermonuclear flash in this model is shown in Figure 9. The helium flash begins at a smaller elapsed time ( $t_R \approx 3.3$  hours) than in model 9, largely because of the lack of general relativistic time dilation in model 17. (Note that the accretion rate as measured by a distant observer is, by assumption, identical in the two models.) As a result of the absence of gravitational redshift, the peak luminosity ( $L_{m1} \approx 1.0 \times 10^{39}$  ergs  $s^{-1}$ ), peak effective temperature ( $T_{em} \approx 2.4 \times 10^7$  K), and emitted burst energy ( $E_b \approx 1.4 \times 10^{39}$  ergs) are all higher than in model 9, despite the smaller recurrence time, and the burst

duration ( $\tau_d \approx 16$  s) is shorter than in model 9. The burst shape is different from that of model 9; since the pressure at the base of the accreted matter in the nonrelativistic model is relatively low, the luminosity maxima resulting from the helium flash and the subsequent rapid hydrogen burning are blended into a single, relatively broad peak. General relativistic effects directly increase the accretion-driven luminosity by a factor of  $2z_s(1+z_s)/[(1+z_s)^2 - 1]$  (see eqs. [3], [15], and [16]), while the peak burst luminosity is decreased by a factor of roughly  $(1+z_s)^{-2}$  (see eq. [16]). Largely as a result of these correction factors, the  $\alpha$ -value in model 17 ( $\alpha \approx 70$ ) is smaller than in model 9.

## VI. DISCUSSION

### a) Equilibrium Core Temperatures

By use of the procedure described in § II, we have estimated the equilibrium core temperature,  $T_{eq}$ , at three values of  $\dot{m}$  ( $1 \times 10^{16}$ ,  $3 \times 10^{16}$ , and  $1 \times 10^{17}$  g  $s^{-1}$ ), both for the case of no neutrino emission by the core and for the case where neutrino emission is given by equation (1) with  $(1+z_c)/(1+z_s) = 2.12$ . For  $\dot{m} = 1 \times 10^{16}$  g  $s^{-1}$ , we applied our interpolation method (see eq. [2]) to model 6 and to a cruder model calculation, corresponding to a core temperature of  $T_c = 9 \times 10^7$  K, which was insufficiently accurate to determine the detailed properties of the emitted X-ray burst but adequate to determine the time-averaged heat flow into the core. For  $\dot{m} = 3 \times 10^{16}$  g  $s^{-1}$  we used the computed results for models 1 and 9, while for  $\dot{m} = 1 \times 10^{17}$  g  $s^{-1}$  we used model 5 and a cruder model calculation corresponding to  $T_c = 1.94 \times 10^8$  K.

The resulting estimates for  $T_{\text{eq}}$  are shown in Figure 2. For a core neutrino emission rate given by equation (1) (i.e.,  $L_\nu = L_\nu^{(1)}$ ), our results can be expressed by the fitting formula

$$T_{\text{eq}} \approx 1.20 \times 10^8 (1 + 0.55x - 0.22x^2) \text{ K},$$

$$1 \times 10^{16} \lesssim \dot{m} \lesssim 1 \times 10^{17} \text{ g s}^{-1}, \quad L_\nu = L_\nu^{(1)}, \quad (22)$$

where  $x \equiv \log(\dot{m}/10^{16} \text{ g s}^{-1})$ , while for  $L_\nu = 0$  our results can be expressed as

$$T_{\text{eq}} \approx 1.47 \times 10^8 (1 + 0.54x + 0.31x^2) \text{ K},$$

$$1 \times 10^{16} \lesssim \dot{m} \lesssim 1 \times 10^{17} \text{ g s}^{-1}, \quad L_\nu = 0. \quad (23)$$

Lamb and Lamb (1978) were the first to point out that a neutron star undergoing accretion at a constant average rate will achieve an equilibrium core temperature. Their estimate for  $T_{\text{eq}}$  (in the case of an unmagnetized neutron star) is also shown in Figure 2. It is now apparent, however, that this estimate is actually an upper limit, for two reasons:

1. Lamb and Lamb (1978) estimated the equilibrium conditions by taking  $\bar{L} = \bar{L}_{\text{nuc}}$ , where  $\bar{L}$  and  $\bar{L}_{\text{nuc}}$  are the time-averaged photon luminosity emitted from the neutron star surface and the time-averaged nuclear luminosity generated in the surface layers, respectively. This is equivalent to the assumption that during the quiescent period of duration  $t_R$  between two thermonuclear flashes, the core loses an amount of energy  $\bar{L}t_R = \bar{L}_{\text{nuc}}t_R = \Omega\Delta M$ , where  $\Omega$  is the energy released per unit rest mass of nuclear fuel (as measured by a distant observer) and  $\Delta M$  is the amount of rest mass that accretes between flashes. Hence, in order for the core to remain in thermal equilibrium, all of the nuclear energy released in each flash should flow into the core. However, it has now been found both in the present numerical calculations and in earlier work (Joss 1978; Joss and Li 1980) that at least  $\sim 80\%$  of the nuclear energy released is promptly emitted from the neutron star surface.

2. Lamb and Lamb (1978) neglected neutrino emission from the core. Indeed, in the absence of general relativistic effects, the core is expected to be roughly isothermal, and for core temperatures less than  $\sim 3 \times 10^8$  K the neutrino luminosity from the core,  $L_\nu$ , is negligible compared to the combined radiative and conductive luminosities (Tsuruta 1979). However, as discussed in § II, general relativistic effects can substantially increase the central temperature of the neutron star as measured by a local observer, relative to the value of  $T_c$  as measured by an observer on the neutron star surface (Glen and Sutherland 1980; Van Riper and Lamb 1981), even though any given observer still finds the core to be isothermal.  $L_\nu$  is then strongly enhanced due to its high sensitivity to (locally measured) temperature (Tsuruta

1979 and references therein). This is especially true for neutron star models based on soft nuclear-matter equations of state (such as those that underlie most of our model calculations), whose central-to-surface gravitational redshifts can exceed 2 (Glen and Sutherland 1980; see § II of the present paper). Hence one cannot neglect  $L_\nu$  for a large range of the core temperatures that we consider ( $T_c > 1 \times 10^8$  K as measured by an observer on the neutron star surface). It is apparent in Figure 2 that our present results more nearly match the estimate by Lamb and Lamb (1978) when we assume that  $L_\nu = 0$ .

We find that whenever  $T_c \lesssim 2 \times 10^8$  K, heating by nuclear burning in the surface layers between nuclear flashes is more important in determining the thermal structure of those layers than the heat outflow from the core. However, for lower core temperatures the heat outflow from the core still plays a significant role in determining the thermal structure of the surface layers. Since we have preferentially considered models with core temperatures near our own estimates of the equilibrium values, nuclear burning between flashes dominates the thermal structure of the surface layers in most of our models. The models calculated by Joss (1978) and Joss and Li (1980) used considerably higher core temperatures, derived from a modified version of Lamb and Lamb's (1978) estimate of the equilibrium values, and their thermal structure was therefore dominated by heat flow from the core. In two of the models calculated by Taam (1981*a*), the assumed core temperatures were also sufficiently high that the heat flow from the core dominated the thermal structure of the surface layers. However, most of the models calculated by Taam and Picklum (1979) and Taam (1980, 1981*a*) assumed relatively low core temperatures ( $T_c \approx 1 \times 10^8$  K; Taam 1981*b*), so that the heat flow from the core was comparatively unimportant. When these differences in assumptions concerning the core temperatures are taken into account, many of the differences in the thermal structure and concomitant properties of the surface layers among the various calculations are readily reconciled.

#### b) General Relativistic Effects

The influence of general relativistic corrections to the equations of stellar structure and evolution was discussed in § V above (see especially § Ve). While many of these effects can be easily understood in terms of the gravitational redshift from the neutron star surface to a distant observer, others seem to be inextricably entwined in the rather complex corrections to the full set of equations (see § III). For the neutron star mass ( $M = 1.41 M_\odot$ ) and radius ( $R = 6.57$  km) that we employed in most of our models, corresponding to a soft nuclear-matter equation of state (Baym, Pethick, and Sutherland 1971), the general relativistic corrections are quite large. For example, by use of equation (3) we find

that the correction to the right-hand side of the equation of hydrostatic equilibrium (eq. [6]) is 2.7—hardly a small effect! However, for neutron stars with larger radii and/or smaller masses, corresponding to the stiffer nuclear-matter equations of state that are more widely accepted at present (see Baym and Pethick 1979 for a review), the general relativistic corrections will be appreciably smaller (see the discussion of models 13 and 14 in § Vd).

In their numerical calculations of neutron star thermonuclear flashes, Taam and Picklum (1979) and Taam (1980, 1981a) included the general relativistic correction to the equation of hydrostatic equilibrium (eq. [6]). However, other general relativistic corrections were not included in a self-consistent manner (Taam 1981b). Other workers (e.g., Czerny and Jaroszyński 1980; Ergma and Tutukov 1980; Fujimoto, Hanawa, and Miyaji 1980) who included general relativistic effects did not carry out fully time-dependent calculations. Hence, the present calculations of neutron star thermonuclear flashes are the first to employ, in a self-consistent manner, all of the significant general relativistic corrections to the stellar structure and evolution equations.

#### c) *The Nuclear Reaction Network*

We have found that our simplified nuclear reaction network adequately approximates the nuclear burning time scales and energetics obtained with more elaborate networks (see § IV). The most serious uncertainty in our network (and in any such network) is the lack of information on the  $\beta$ -decay time scales of the highly proton-rich nuclei that participate in the  $rp$  process. As shown by Taam (1981a), reasonable variations in the assumed  $\beta$ -decay time scales can produce significant changes in the properties of X-ray bursts resulting from neutron star thermonuclear flashes.

We also note that the assumed value of the initial heavy-element abundance by mass,  $Z$ , of the accreting matter has a significant impact upon the nuclear burning processes prior to and during a neutron star thermonuclear flash. We took  $Z = 10^{-2}$  in most of our model calculations. However, there is considerable evidence by now that many, if not all, X-ray burst sources are Population II objects (see Lewin and Joss 1981 for references), for which  $Z \lesssim 10^{-3}$  would be a more plausible assumption. Also potentially important in this regard is the gravitational settling of heavy elements in the intense surface gravity of a neutron star (see, e.g., Alcock and Illarianov 1980), which could lower the effective value of  $Z$  in the freshly accreted matter.

#### d) *Shell Separation, Flash Suppression, and Scaling Relations*

In some of the models described in § V, the helium-burning shell becomes separated below the hydrogen-

burning shell before the onset of a thermonuclear flash, while in other models the two shells still overlap when the flash commences. The presence or absence of overlapping shells has important consequences for the properties of the flashes. In particular, if hydrogen is present in an overlapping shell during a helium flash, the nuclear energy per unit mass available in the subsequent rapid nuclear burning is considerably larger than if the shells have separated. As we shall now show, it is possible to formulate a simple criterion to determine whether the shells will separate in a given case.

The requirement for shell separation is that the hydrogen at the base of the freshly accreted matter must be consumed by quiescent nuclear burning before a helium flash commences. This situation will occur only if the recurrence time between flashes is sufficiently long. Specifically, for shell separation to occur we require that

$$\dot{m} \leq \frac{\epsilon_{\text{CNO}} \Delta M}{E_{\text{H}}(1+z_s)}; \quad (24)$$

or, since  $\Delta M = \dot{m} t_R$ ,

$$t_R \geq \frac{E_{\text{H}}(1+z_s)}{\epsilon_{\text{CNO}}} \\ \approx 1.3 \times 10^5 \left( \frac{X}{0.7} \right) \left( \frac{Z_{\text{CNO}}}{10^{-2}} \right)^{-1} \left( \frac{1+z_s}{1.65} \right) \text{ s} \quad (25)$$

(see also Taam 1981a). Here  $\dot{m}$  is the accretion rate,  $\epsilon_{\text{CNO}}$  is the hydrogen-burning rate via the saturated CNO cycle (see eq. [21]), which is usually the relevant rate during quiescent hydrogen burning,  $Z_{\text{CNO}}$  is the fractional abundance, by mass, of the heavy elements that participate in the cycle,  $X$  is the fractional abundance of hydrogen by mass, and  $E_{\text{H}} \approx 4.5 \times 10^{18} (X/0.7)$  ergs  $\text{g}^{-1}$  is the nuclear energy per unit mass released in hydrogen burning. (Note that both  $\epsilon_{\text{CNO}}$  and  $E_{\text{H}}$  are as measured by an observer on the neutron-star surface.)

We can also roughly estimate the value of  $\Delta M$  from the following argument. If the saturated CNO cycle is the dominant source of heat input to the freshly accreted matter (so that, in particular, the heat flow from the neutron star core is negligible), and if an approximate balance is maintained between the energy generated in this matter and the luminosity  $L_0$  (as measured by a local observer) propagating outward toward the neutron star surface, then

$$L_0 \approx \epsilon_{\text{CNO}} \Delta M. \quad (26)$$

Since the surface layers are generally not convective during quiescent burning, we can combine equation (26) with equation (5) and the form of equation (8) appropriate to radiative zones. After making some

straightforward approximations and some algebraic manipulation, we obtain

$$\Delta M \approx 4\pi \left[ \frac{2}{3} \frac{ac}{\bar{\kappa} \epsilon_{\text{CNO}}} \right]^{1/2} R^2 T_b^2, \quad (27)$$

where  $\bar{\kappa}$  is the mass-averaged value of the combined radiative and conductive opacity in the surface layers and  $T_b$  is the temperature at the base of the freshly accreted matter. If we further take the nuclear flash to begin at the time when the energy generation rate from helium-burning reactions,  $\epsilon_{\text{He}}$ , exceeds  $\epsilon_{\text{CNO}}$ , then the strong energy dependence of  $\epsilon_{\text{He}}$  allows us to assign a unique temperature of  $\sim 2 \times 10^8$  K to  $T_b$  at the start of the flash. Thus, substituting numerical values into equation (27), we find that

$$\begin{aligned} \Delta M &\approx 6 \times 10^{20} \left( \frac{\bar{\kappa}}{0.4 \text{ cm}^2 \text{ g}^{-1}} \right)^{-1/2} \\ &\times \left( \frac{Z_{\text{CNO}}}{10^{-2}} \right)^{-1/2} \left( \frac{R}{6.57 \text{ km}} \right)^2 \left( \frac{T_b}{2 \times 10^8 \text{ K}} \right)^2 \text{ g}. \end{aligned} \quad (28)$$

By combining equation (28) with relation (24) and equation (21), we can obtain a condition for shell separation to occur in terms of the accretion rate:

$$\begin{aligned} \dot{m} &\lesssim 4 \times 10^{15} \left( \frac{X}{0.7} \right)^{-1} \left( \frac{1+z_s}{1.65} \right)^{-1} \left( \frac{\bar{\kappa}}{0.4 \text{ cm}^2 \text{ g}^{-1}} \right)^{-1/2} \\ &\times \left( \frac{Z_{\text{CNO}}}{10^{-2}} \right)^{-1/2} \left( \frac{R}{6.57 \text{ km}} \right)^2 \left( \frac{T_b}{2 \times 10^8 \text{ K}} \right)^2 \text{ g s}^{-1}. \end{aligned} \quad (29)$$

Relation (29) is evidently consistent with the results of our numerical calculations. In model 2, for which  $\dot{m} = 1 \times 10^{15}$  g s<sup>-1</sup>, shell separation occurs prior to the start of a flash; in model 3, for which  $\dot{m} = 3 \times 10^{15}$  g s<sup>-1</sup>, the shells just marginally separate prior to the flash. In all other models, for which  $\dot{m}$  is at least  $1 \times 10^{16}$  g s<sup>-1</sup>, no shell separation occurs. Criterion (29) is also consistent with our results for models that assumed values for  $Z_{\text{CNO}}$  and  $R$  which differ from the standard values used above.

We can use a similar argument to estimate roughly the conditions under which subsequent thermonuclear flashes will be suppressed after the first flash following the onset of accretion. After most of the nuclear energy of a flash has been released, the time scale, as measured by a distant observer, for the cooling of the burning shell from temperature  $T_1$  to temperature  $T_2$  is given by

$$t_{\text{cool}} \approx (1+z_s) \int_{T_1}^{T_2} \frac{C_p \Delta M}{L_0} dT.$$

Here  $C_p \approx 10^8$  ergs g<sup>-1</sup> K<sup>-1</sup> is the specific heat at constant pressure (which we assume, for simplicity, to be spatially and temporally constant) and  $\Delta M$  is again the rest mass of the freshly accreted matter (which we take to be about equal to the amount of mass in the burning shell). As before, we neglect the heat flow, if any, from the neutron star core. If we again estimate  $L_0$  from equation (5) and the form of equation (8) appropriate to radiative equilibrium (which is restored on a time scale of  $\lesssim 5$  s following a flash), we obtain

$$t_{\text{cool}} \approx - \frac{3C_p \bar{\kappa} \Delta M^2 (1+z_s)}{16\pi^2 ac R^4} \int_{T_1}^{T_2} \frac{dT}{T^4}.$$

Carrying out the integral, taking  $T_1$  to be the peak temperature at the base of the shell following the flash and  $T_2$  to be the temperature at which helium-burning becomes important ( $\sim 2 \times 10^8$  K), making the approximation that  $T_2 \ll T_1$ , and substituting the same numerical values that were used in equations (28) and (29), we obtain

$$\begin{aligned} t_{\text{cool}} &\approx \frac{C_p \bar{\kappa} \Delta M^2 (1+z_s)}{16\pi^2 ac R^4 T_2^3} \\ &\approx 4 \times 10^2 \left( \frac{\Delta M}{6 \times 10^{20} \text{ g}} \right)^2 \text{ s}. \end{aligned} \quad (30)$$

Indeed, the temperature must stay below  $T_2 \approx 2 \times 10^8$  K in order that freshly accreting helium not be consumed by nuclear burning as rapidly as it accumulates. Hence, if after a flash  $t_{\text{cool}}$  is smaller than the accretion time scale,

$$\begin{aligned} t_{\text{acc}} &\equiv \frac{\Delta M}{\dot{m}} \\ &\approx 2 \times 10^4 \left( \frac{\dot{m}}{3 \times 10^{16} \text{ g s}^{-1}} \right)^{-1} \left( \frac{\Delta M}{6 \times 10^{20} \text{ g}} \right) \text{ s}, \end{aligned} \quad (31)$$

then the surface layers are able to cool sufficiently to allow helium to accumulate, and no further flashes will occur. By comparison of equations (30) and (31), we find that  $t_{\text{cool}} < t_{\text{acc}}$  when

$$\begin{aligned} \dot{m} &\lesssim \frac{16\pi^2 ac R^4 T_2^3}{C_p \bar{\kappa} \Delta M (1+z_s)} \\ &\approx 2 \times 10^{18} \left( \frac{\Delta M}{6 \times 10^{20} \text{ g}} \right)^{-1} \text{ g s}^{-1}. \end{aligned} \quad (32)$$

Actually, relation (32) somewhat overestimates the maximum value of  $\dot{m}$  for which subsequent flashes will

not be suppressed, since at relatively high accretion rates the cooling time scale will be increased by the release of nuclear energy via hydrogen burning. From arguments similar to those presented above, we estimate that the cooling time scale can be significantly increased when  $\dot{m} \gtrsim 10^{17} \text{ g s}^{-1}$ . Moreover, at accretion rates still higher than the critical value estimated in relation (32), compressional heating of the surface layers by the infalling matter can cause the helium to be consumed as fast as it accumulates, and can thereby prevent the occurrence of even the initial flash after the onset of accretion. Similarly, if the core temperature of the neutron star is very high, the helium will be consumed as rapidly as it is accreted, and no flashes will occur.

These estimates are again consistent with the results of our numerical evolutionary calculations (see Table 2). For  $\dot{m} \leq 10^{17} \text{ g s}^{-1}$  there is no evidence for suppression of the first flash. However, our preliminary results for the second flash in our standard model (see § Va) indicate that the time interval between the first and second flashes is less than half as long as the time interval between the onset of accretion and the first flash. The second flash is accordingly weaker than the first, due to the smaller amount of available nuclear fuel. These effects can be traced directly to the elevated temperatures in the surface layers following the first flash (i.e., partial suppression of the second flash apparently occurs even for accretion rates as low as  $3 \times 10^{16} \text{ g s}^{-1}$ ). For  $\dot{m} = 3 \times 10^{18} \text{ g s}^{-1}$ , the compressional heating the surface layers partially suppresses even the first flash, and the first flash is completely suppressed for  $\dot{m} = 3 \times 10^{19} \text{ g s}^{-1}$ . The first flash is also partially or completely suppressed at the highest core temperature that we consider,  $T_c = 5.7 \times 10^8 \text{ K}$ .

In view of the above considerations, it is clear that the time interval between the onset of accretion and the initial flash, which we have called the recurrence time ( $t_R$ ) in § V and Table 2, is not necessarily the time interval between any two successive flashes. For  $\dot{m} \lesssim 1 \times 10^{16} \text{ g s}^{-1}$  the recurrence intervals in any given model should be relatively uniform (and about equal to our values of  $t_R$ ), but at higher accretion rates there may be complex variations in the recurrence intervals between successive flashes. We are presently investigating such variations and shall report our results elsewhere (see also the comments at the end of § VIe below).

Joss and Li (1980) showed that their results for pure helium flashes could be expressed in terms of simple scaling relations involving the neutron star mass and radius. Similar relations should apply to models calculated under the less restrictive approximations made in the present paper, provided that the hydrogen-burning and helium-burning shells separate prior to a helium flash. However, the relations given by Joss and Li (1980) must be modified as follows: (1) Joss and Li employed sufficiently high values for  $T_c$  that the heat outflow from

the core dominated the thermal structure of the surface layers. In cases where the thermal structure is, instead, controlled by nuclear energy generation in the surface layers, then  $\Delta M$  must be estimated by use of equation (28). (2) The general relativistic corrections to the equations of stellar structure and evolution (see § III) must be taken into account. In particular, the general relativistic Eddington limit (as measured by a distant observer),

$$L_{\text{ed}}^{(R)} = \frac{4\pi cGM}{\kappa_T(1+z_s)} \\ \approx 1.26 \times 10^{38} \left( \frac{M}{1.41 M_\odot} \right) \left( \frac{1+X}{1.69} \right)^{-1} \\ \times \left( \frac{1+z_s}{1.65} \right)^{-1} \text{ ergs s}^{-1}, \quad (33)$$

is lower than the Newtonian value by a factor of  $(1+z_s)$ , so that the Eddington limit depends on both the mass and the radius of the neutron star. [In eq. (33),  $\kappa_T \approx 0.20(1+X) \text{ cm}^2 \text{ g}^{-1}$  is the Thomson scattering opacity at the neutron star surface.]

We have carried out full calculations for only one model (model 3) wherein the hydrogen-burning and helium-burning shells separated, so that we are unable to confirm the validity of scaling relations of the type advocated by Joss and Li (1980). In cases where the shells overlap at the time of the helium flash, the complex behavior of the interacting shells evidently precludes the formulation of scaling relations of comparable simplicity. In particular, although the peak luminosity following a thermonuclear flash is still generally of the order of the Eddington limit (see Joss 1977), the ratio of the peak luminosity to the Eddington limit varies by up to a factor of  $\sim 4$  in our models (even if we disregard the contribution of the accretion-driven luminosity, whose dynamical effects are neglected in our calculations).

#### e) Unburned Fuel and Residual Radioactivity

Two mechanisms that might produce further differences among successive thermonuclear flashes, in addition to the flash suppression process discussed in the preceding subsection, are the incomplete burning of the available nuclear fuel in a flash (Lamb and Lamb 1978) and the release of energy by the residual radioactivity of the burned fuel. All of these mechanisms could contribute to irregularities in the recurrence intervals between observed bursts from type I X-ray burst sources, which, in extreme cases, have been as short as  $\sim 10$  minutes (Lewin *et al.* 1976; Murakami *et al.* 1980). In the following paragraphs, we shall discuss the effects of incomplete fuel consumption and residual radioactivity in the light of our model calculations. In § VII, we shall briefly

discuss some other mechanisms that might contribute to the observed differences among successive X-ray bursts.

The model (see § V and Table 2) that had the largest amount of unburned nuclear fuel was model 16 (which had a lower initial heavy element abundance,  $Z = 10^{-3}$ , than that of the standard model); the fractional abundance by mass of unburned hydrogen in the surface layers at a time 100 s after the start of the flash in this model was 0.40. The reason for the large amount of unburned fuel in this case is the relatively high hydrogen abundance and low helium abundance just prior to the flash, which results directly from the low metallicity and the concomitantly slow rate of hydrogen burning before the flash. Because of the low helium abundance, relatively few seed nuclei for the  $rp$  process are synthesized by the helium flash. In addition, the high peak shell-burning temperature,  $T_{\text{bm}} \approx 2 \times 10^9$  K, causes  $(\alpha, p)$  reactions to play a major role in the  $rp$  process (see § IV) and thereby further reduces the consumption of hydrogen. The amount of unburned hydrogen could cause substantial differences in the properties of subsequent flashes with respect to those of the first flash, and approaches the amount needed to account for the shortest observed intervals between type I X-ray bursts. This result is very suggestive, since model 16 is the only model that we have calculated for which Population II abundances were assumed for the accreting material. We caution, however, that we stopped the numerical calculations  $\sim 100$  s after the first flash, and we cannot exclude the possibility that a significant amount of rather rapid hydrogen burning consumes much of the residual hydrogen on a time scale in excess of  $\sim 100$  s but less than the burst recurrence time. Another potentially important effect (see, e.g., Alcock and Illarianov 1980) that must be quantitatively investigated in this context is the gravitational settling of CNO nuclei from freshly accreting material into the zone containing residual hydrogen. Since nearly all of the ambient CNO nuclei should be consumed during the flash, such settling may strongly alter the nuclear reaction rates within this zone. We are now investigating the behavior of such models at later times following the initial flash, and we shall report our results elsewhere.

The burned fuel will be radioactive due to the  $\beta$ -instability of the proton-rich nuclei, especially  $^{56}\text{Ni}$  and  $^{56}\text{Co}$ , that are produced by the  $rp$  process (see § IV). The  $^{56}\text{Ni}$  and  $^{56}\text{Co}$  nuclei are particularly important, since their decay, which releases 2.1 and 4.6 MeV per nucleus, respectively, will proceed on time scales comparable to the intervals between thermonuclear flashes. The energy released by the radioactive decay of  $^{56}\text{Ni}$  and  $^{56}\text{Co}$  can thus alter the thermal properties of the neutron-star surface layers between flashes and thereby vary the behavior of successive flashes.

Positron decay from the ground state of  $^{56}\text{Ni}$  is highly forbidden, and terrestrially this species decays into  $^{56}\text{Co}$

via K-shell electron capture. In the surface layers of a neutron star, the decay will proceed via the capture of continuum electrons at temperatures less than  $\sim 10^9$  K and via positron decays from thermally populated excited states at higher temperatures. From the decay rates given by Fuller, Fowler, and Newman (1981), we have devised a simple fitting formula for the resultant energy generation rate,  $\epsilon_{\text{Ni}}$ , when conditions are in the range of  $10^3 \lesssim \rho \lesssim 10^7$  g cm $^{-3}$  and  $T \lesssim 10^9$  K:

$$\epsilon_{\text{Ni}} \approx 1.26 \times 10^{10} X_{\text{Ni}} 10^{y(0.155y-0.625)} \text{ ergs g}^{-1} \text{ s}^{-1},$$

$$y \equiv \log(\rho/\mu_e). \quad (34)$$

Here,  $X_{\text{Ni}}$  is the fractional abundance, by mass, of  $^{56}\text{Ni}$ ,  $\mu_e$  is the mean molecular weight per electron,  $\rho$  is in units of g cm $^{-3}$ , and we have assumed, based on calculations by Fuller, Fowler, and Newman (1981), that an average of 0.6 MeV per decay is lost to the emitted neutrinos.

The  $^{56}\text{Co}$  daughter nuclei will also undergo  $\beta$ -decay (into  $^{56}\text{Fe}$ ). From the rates given by Fuller, Fowler, and Newman (1981), we have devised a fitting formula for the resultant energy generation rate,  $\epsilon_{\text{Co}}$ , when conditions are in the range of  $10^3 \lesssim \rho \lesssim 10^6$  g cm $^{-3}$  and  $3 \times 10^8 \lesssim T \lesssim 10^9$  K (in which case the decay rate is dominated by positron decays from excited states):

$$\epsilon_{\text{Co}} \approx 1.16 \times 10^{10} X_{\text{Co}} 10^{2.8(T/10^8 \text{ K})} \text{ ergs g}^{-1} \text{ s}^{-1}. \quad (35)$$

Here  $X_{\text{Co}}$  is the fractional abundance, by mass, of  $^{56}\text{Co}$ , and we have assumed, based on calculations by Fuller, Fowler, and Newman (1981), that 2.0 MeV per decay is lost to the emitted neutrinos. At higher densities and temperatures than those within the range of validity of equation (35), the decay of  $^{56}\text{Co}$  is so rapid that it will not be important during the intervals between thermonuclear flashes, but will instead contribute slightly to the energy released by rapid nuclear burning immediately following a flash. For  $\rho \lesssim 10^6$  g cm $^{-3}$  and  $T \lesssim 2 \times 10^8$  K, the decay rate of  $^{56}\text{Co}$  is too slow to be of interest in the present context.

Other  $\beta$ -unstable nuclei that participate in the  $rp$  process and the CNO cycle generally decay too quickly to influence the thermal structure of the surface layers between flashes. However, the decay of such nuclei contributes to the energetics of the X-ray bursts themselves, and these decays should therefore be taken into account in the nuclear reaction network (see §§ IV and Va).

In order to determine the effect of  $^{56}\text{Ni}$  and  $^{56}\text{Co}$   $\beta$ -decay on the thermal history of the neutron star surface layers, we have carried out a preliminary calculation of the evolution of our standard model (see § Va) through a second thermonuclear flash with  $^{56}\text{Co}$  and  $^{56}\text{Fe}$  added to our nuclear reaction network and these

decays taken into account. A considerable amount of  $^{56}\text{Ni}$  was synthesized by the  $rp$  process in the first flash, and we estimated the energy released in its decay and that of the  $^{56}\text{Co}$  daughter nuclei by use of equations (34) and (35). Our results suggest that the second flash occurs after only  $\sim 2.0$  hours have elapsed since the initial flash. This interval is  $\sim 10\%$  shorter than that which we obtained in a preliminary calculation that neglected  $^{56}\text{Ni}$  and  $^{56}\text{Co}$  decay (see § Va), due to a further increase in the temperatures within the surface layers resulting from the extra energy release. We are continuing our exploration of the quantitative effects of residual radioactivity, and we shall report our results elsewhere.

#### f) Effects of Surface Magnetic Fields

If an accreting neutron star has a strong surface magnetic field, there will be at least two important effects upon the accretion process and the resultant thermonuclear processes in the surface layers: (1) the field can funnel the accretion flow onto the magnetic polar caps of the neutron star; and (2) the field can suppress the radiative and conductive opacities in the surface layers. (In § VII, we shall briefly discuss a few other consequences that strong surface fields might have.) We shall discuss these two effects in the following paragraphs.

If the neutron star magnetic field is sufficiently strong, it will funnel the accretion flow onto polar caps whose surface area is probably only  $\sim 10^{-3}$  that of the total surface area of the neutron star (Lamb, Pethick, and Pines 1973). The value of the typical surface field strength,  $B$ , required to produce such funneling is presently uncertain, but the available theoretical work (Arons and Lea 1980) suggests that  $B$  should be at least  $\sim 10^{12}$  gauss. When such funneling takes place, the results of our evolutionary calculations, wherein spherical symmetry was assumed, can be scaled to take the effects of funneling into account (Joss and Li 1980). In particular, the effective accretion rate onto the polar caps will exceed the accretion rate integrated over the entire neutron star surface by a factor of  $\zeta^{-1}$ , where  $\zeta \approx 10^{-3}$  is the fractional surface area of the caps. Thus, for our standard model, wherein  $\dot{m} = 3 \times 10^{16} \text{ g s}^{-1}$ , the effective accretion rate onto the polar caps will be  $\dot{m}\zeta^{-1} \approx 3 \times 10^{19} \text{ g s}^{-1}$ . From the results of model 7 (see § Vd), which has the same parameter values as the standard model except that  $\dot{m} = 3 \times 10^{19} \text{ g s}^{-1}$ , and from the arguments presented in § VI d above, we conclude that thermonuclear flashes will be completely suppressed at such high accretion rates. (See Joss and Li 1980 for a more complete discussion of the scaling of results for spherically symmetric models to take magnetic funneling into account.)

The reduction of the radiative and conductive opacities in the neutron star surface layers by a strong mag-

netic field will also tend to suppress flashes (Joss and Li 1980). Model 15 had the same parameter values as those of our standard model, except that the opacities were reduced by an amount appropriate to a surface field strength of  $3 \times 10^{12}$  gauss (see § Vd). This is the same field strength that was assumed in model *b* by Joss and Li (1980), and the effects of the strong field were similar: the suppression of opacities resulted in more efficient heat transport away from the nuclear burning shell, smaller temperature gradients in the surface layers, longer intervals between thermonuclear flashes, and concomitantly stronger X-ray bursts (due to the larger amounts of fuel stored in the surface layers between flashes). In practice, the suppression of the conductive opacity was much more important than that of the radiative opacity. Joss and Li (1980) found that flashes were suppressed entirely by surface fields in excess of  $\sim 1 \times 10^{13}$  gauss; we have not recalculated any models with such intense fields, but we expect that flashes probably would again be completely suppressed for  $B \gtrsim 10^{13}$  gauss. (Note that the assumption of a uniform magnetic field that is everywhere perpendicular to the neutron star surface, as was employed in model 15, is probably a valid approximation for the magnetic polar caps onto which the accretion flow should be funneled.)

In summary, we expect, on the basis of our evolutionary calculations, that a strong surface magnetic field can completely suppress neutron star thermonuclear flashes by funneling the accretion flow and/or by reducing the radiative and conductive opacities in the surface layers. This result strengthens the argument (see Taam and Picklum 1978; Joss 1978; Joss and Li 1980) that the dichotomy between type I X-ray burst sources and X-ray pulsars results from differences in the surface magnetic field strengths of the accreting neutron stars. In this picture, the type I burst sources are accreting neutron stars that are relatively weakly magnetized and whose nuclear burning shells can therefore undergo thermonuclear flashes; the X-ray pulsars are presumably more strongly magnetized neutron stars wherein the accretion flow is funneled onto the magnetic polar caps, giving rise to X-ray pulsations as the neutron star rotates, and wherein the nuclear burning shells are stabilized by the strong field.

#### VII. CONCLUDING REMARKS

The models for the evolution of the surface layers of accreting neutron stars that we have calculated include the most complete physics that has yet been attempted in any such models. Specifically, our models took into account the detailed heat flow into and out of the neutron star core, included all significant general relativistic effects, and incorporated a nuclear reaction network that adequately describes all major hydrogen-burning and helium-burning reactions. Moreover, our 17 principal models span a wide range of the space of

parameters describing the accreting matter and the underlying neutron star.

The X-ray bursts that result from thermonuclear flashes in our models (see Table 2 and Figs. 3, 6, 7, and 8) are consistent with most of the properties of observed type I X-ray bursts (Lewin and Joss 1981 and references therein). In particular, we are able to reproduce the typical burst rise times, peak luminosities, blackbody temperatures, decay time scales, total emitted energies, and recurrence intervals, as well as the typical ratios of average persistent X-ray luminosity to time-averaged burst luminosity from burst sources. It is therefore tempting to attempt a detailed comparison of some of the features of our results with specific observational properties of type I bursts. However, as will be documented below, there are at present several significant discrepancies between some characteristics of at least a few type I burst sources and the predictions of the thermonuclear flash model. We believe that it is premature to carry out any detailed comparisons between theory and observation, at least until the sources of discrepancy are more clearly identified.

The principal discrepancies between the thermonuclear flash model and observational properties of type I burst sources are as follows:

1. The peak luminosities of the X-ray bursts from a few type I burst sources appear to exceed the Eddington limit (see eq. [33]) by factors of  $\sim 3$ – $10$  (Grindlay *et al.* 1980; Grindlay and Hertz 1981; Inoue *et al.* 1980 and references therein). However, the peak burst luminosity was always less than the Eddington limit in the present model calculations, as expected on the basis of theoretical considerations discussed by Joss (1977, 1978). (Some of the models calculated by Taam 1980, 1981*a* have peak surface luminosities in excess of the Eddington limit. However, according to Taam 1981*b* the reported surface luminosities are not the actual photon luminosities from the neutron star photosphere, so that the physical significance of these super-Eddington luminosities is unclear.) Some of this discrepancy would be removed if the distances to the relevant sources were found to have been overestimated, but it seems unlikely that such observational errors could account for the entire effect.

2. The peak effective temperatures observed in some type I bursts (up to  $\sim 3 \times 10^7$  K) exceed the theoretical maximum value ( $T_0 \approx 2.1 \times 10^7$  K) for spherically symmetric emission by a neutron star radiating at less than the Eddington limit, when general relativistic effects are taken into account (see Goldman 1979; van Paradijs 1979; Marshall 1981). The maximum effective temperatures that were reached in our general relativistic model calculations are all less than the theoretical maximum (provided that the artificially high effective temperatures resulting from very high accretion rates are excluded); the highest value that we obtained was  $\sim 1.9 \times 10^7$  K (in

model 5). This difficulty is more fundamental than the apparent super-Eddington luminosities themselves, since the measured effective temperatures are independent of the assumed source distances.

3. The apparent radius of the X-ray emitting surface is occasionally observed to first increase and then decrease by a factor of several during type I burst events (Swank *et al.* 1977; Grindlay *et al.* 1980; Hoffman, Cominsky, and Lewin 1980 and references therein). In contrast, the photospheric radius of the neutron star remains nearly constant during burst emission in the present model calculations. Cominsky (1981) has suggested that the apparent radius changes might result from reprocessing of some of the X-ray flux by other matter in the vicinity of the neutron star, but the viability of this idea has not yet been explored.

All other apparent discrepancies between the predictions of the thermonuclear flash model and the observed properties of type I burst sources (Lewin and Joss 1981 and references therein; see also § VI above) seem to be more easily reconcilable than these three. In the following paragraphs, we shall discuss the potential relevance of several mechanisms, none of which have yet been included in detailed evolutionary model calculations of X-ray bursts, to the resolution of these difficulties.

Dynamical phenomena in the neutron star surface layers could, in principle, alleviate all three difficulties by generating luminosities in excess of the Eddington limit (which would, in turn, allow the maximum effective temperatures to exceed  $T_0$ ) and by causing the neutron star photosphere to expand. The energy released in a neutron star thermonuclear flash is always insufficient to cause a breakdown of hydrostatic equilibrium throughout the surface layers (Joss 1978), but dynamical effects might still be important in an outermost layer of small fractional mass. However, in our model calculations the time scale for release of energy in a thermonuclear flash is always several orders of magnitude longer than the sound travel time across the surface layers, so that the generation of energetically significant shock waves seems unlikely. Taam (1981*a*) reported the development of dynamical effects in the outer surface layers of one of his models, but no details of his results were given. Wallace, Woosley, and Weaver (1981) have carried out dynamical calculations of a model wherein the energy release was a factor of  $\sim 10^2$  larger than in a typical X-ray burst; they found that the luminosity increased to about the Eddington limit (but not higher) and that the generation of a strong stellar wind caused the photospheric radius to increase by a factor of several during the subsequent X-ray outburst (which lasted for  $\sim 300$  s). As a result of this photospheric expansion, the effective temperature was substantially *lower* than in our models.

We conclude that dynamical phenomena probably will not be of major importance to our understanding of

very high luminosities and effective temperatures in observed X-ray bursts, but that such phenomena may contribute to the observed variations in effective radius. Much more work in the theoretical investigation of dynamical effects remains to be done.

Violations of spherical symmetry on the neutron star surface may contribute to the observed properties of X-ray bursts (Joss 1979; Hōshi 1980). The minimum surface magnetic field strength for which the accretion flow will be funneled onto small magnetic polar caps is uncertain, but available estimates (Arons and Lea 1980) suggest that the accretion will be spread over a large fraction of the neutron star surface if the typical field strength is less than  $\sim 10^{12}$  gauss. However, a relatively weak or chaotic field may still be capable of causing the accretion flow and the structure of the underlying surface layers to differ significantly from complete spherical symmetry. Also, the residual angular momentum of the accreting material may be sufficient to produce significant deviations from spherical symmetry, especially if the accretion onto the surface is mediated by a disk.

Resultant deviations of thermonuclear flashes from spherical symmetry could, in principle, allow the peak luminosity to exceed the Eddington limit, since that limit entails the assumption of spherical symmetry (see, e.g., Basko and Sunyaev 1976). Moreover, if a flash is confined to only a portion of the neutron star surface, then the theoretical limitation on the maximum effective temperature is also not rigorously applicable, even if the luminosity is less than the Eddington limit. However, it is difficult to see how deviations from spherical symmetry could result in any large violations of either the Eddington limit or the restriction on effective temperature. Such deviations may, nonetheless, play an important role in other observed properties of type I bursts. For example, a flash may originate on a limited portion of the stellar surface and propagate around the star, in a pattern that varies from burst to burst in a given source and from one burst source to another. Perhaps most importantly, the isolation of the flash on a fraction of the neutron star surface may provide an additional means of conserving nuclear fuel for future flashes (see Lewin and Joss 1981 and the discussion in § VIe above).

The detailed investigation of violations of spherical symmetry will require two-dimensional or three-dimensional numerical calculations, which will be much more difficult than the calculation of spherically symmetric models. Fryxell and Woosley (1981) have recently carried out a two-dimensional calculation of a neutron star thermonuclear flash, and Woosley and Wallace (1981) recently suggested a mechanism whereby magnetic confinement of material near the neutron star surface following a flash results in effective temperatures in excess of  $T_0$ . However, at the present time the role of violations of spherical symmetry in the observed properties of type I bursts remains unclear.

A moderately strong magnetic field will also tend to suppress the radiative opacity near the neutron star photosphere (Joss and Li 1980; see also §§ Vd and VI above). Hence, the Eddington limit given by equation (33) is no longer applicable and should be replaced by the critical luminosity:

$$L_{\text{crit}} = \frac{\kappa_T}{\kappa_R} L_{\text{ed}} \equiv \Psi_R L_{\text{ed}}, \quad (36)$$

where  $\kappa_R$  is the Rosseland mean value of the suppressed Thomson scattering opacity. Since the luminosity is proportional to the fourth power of the effective temperature, it also follows that  $T_0$  should be replaced by the critical temperature

$$T_{\text{crit}} = \Psi_R^{1/4} T_0. \quad (37)$$

We can roughly estimate the factor by which  $L_{\text{crit}}$  and  $T_{\text{crit}}$  are enhanced by use of equations (5) and (6) in Joss and Li (1980):

$$\begin{aligned} \Psi_R &\approx \frac{5}{4\pi^2} \left( \frac{\hbar\omega_c}{kT} \right)^2 \\ &\approx 22.9 \left( \frac{T}{10^7 \text{ K}} \right)^{-2} \left( \frac{B}{10^{12} \text{ gauss}} \right)^2. \end{aligned} \quad (38)$$

Here  $\hbar$  is Planck's constant divided by  $2\pi$ ,  $k$  is Boltzmann's constant,  $T$  is the temperature as measured by an observer on the neutron star surface, and  $\omega_c$  and  $B$  are typical values of the electron cyclotron angular frequency and magnetic field strength near the surface, respectively.

Equation (38) is based on the Rosseland mean opacity and is thus not strictly valid at the photosphere, but it should be an adequate approximation at moderate optical depths beneath the photosphere. A better approximation near the photosphere is given by the Planck mean. Carrying out a calculation analogous to that in Joss and Li (1980), we obtain

$$\begin{aligned} \Psi_P &\equiv \frac{\kappa_T}{\kappa_P} \approx \frac{21}{40\pi^2} \left( \frac{\hbar\omega_c}{kT} \right)^2 \\ &\approx 9.60 \left( \frac{T}{10^7 \text{ K}} \right)^{-2} \left( \frac{B}{10^{12} \text{ gauss}} \right)^2, \end{aligned} \quad (39)$$

where  $\kappa_P$  is the Planck mean value of the suppressed opacity. Equations (38) and (39) are only valid for  $\Psi_R$  and  $\Psi_P$  greater than unity; when these equations give smaller values, one should instead take  $\Psi_R \approx \Psi_P \approx 1$ . We also emphasize that equations (38) and (39) are based on the assumption that Thomson scattering is the only contributor to the radiative opacity and, in particular, neglect the (uncertain) contributions of cyclotron absorption to the opacity. Moreover, in making these estimates we have neglected the complex angular and mode dependence of the suppressed scattering cross section.

Replacing  $T$  with the effective temperature as measured by a distant observer (see eq. [16]), we estimate

that to enhance  $L_{\text{crit}}$  by a factor of  $\Psi_R$  or  $\Psi_P$  requires a typical surface magnetic field strength of

$$B \approx 0.69 \times 10^{12} \Psi_R^{3/4} \left( \frac{1+z_s}{1.65} \right) \left( \frac{T_e}{2 \times 10^7 \text{ K}} \right) \text{ gauss (Rosseland mean)}$$

$$\approx 1.1 \times 10^{12} \Psi_P^{3/4} \left( \frac{1+z_s}{1.65} \right) \left( \frac{T_e}{2 \times 10^7 \text{ K}} \right) \text{ gauss (Planck mean).} \quad (40)$$

Here,  $T_e$  is the effective temperature, as measured by a distant observer, corresponding to the Eddington limit (uncorrected for opacity suppression). The magnetic field strength needed to enhance  $T_0$  by a factor of  $\Psi_R$  or  $\Psi_P$  can be found by substituting  $T_0$  for  $T_e$  in equation (40). Thus, an enhancement of the critical luminosity and temperature by factors of  $\sim 5$  and  $\sim 1.5$ , respectively, requires surface field strengths of  $\sim 3 \times 10^{12}$  gauss. Whether the accretion flow can be spread over a large fraction of the neutron star surface in the presence of such an intense field, or whether it will instead be confined to small magnetic polar caps, is presently un-

certain. If, however, the accretion flow is not strongly funneled, then the suppression of radiative opacity by the magnetic field is a very promising mechanism to account for the highest observed luminosities and effective temperatures of type I bursts. Clearly, the possible suppression of radiative opacities near the neutron star photosphere by magnetic fields is a problem worthy of further study.

In conclusion, a resolution of the remaining major discrepancies between the observed properties of type I cosmic X-ray bursts and the predictions of the thermonuclear flash model is not yet in hand. However, in view of the continued general agreement between the model and most observational features of type I burst sources, this model remains the most promising available explanation for the type I burst phenomenon.

We acknowledge helpful discussions with L. Cominsky, W. Fowler, J. Heshmati-Moulai, W. Lewin, R. Taam, and S. Woosley. We thank K. Vafa for assistance in developing the nuclear reaction network and S. Pollock for assistance in carrying out the numerical calculations.

## REFERENCES

- Alcock, C., and Illarianov, A. 1980, *Ap. J.*, **235**, 534.  
 Arons, J., and Lea, S. M. 1980, *Ap. J.*, **235**, 1016.  
 Barranco, M., Buchler, J. R., and Livio, M. 1980, *Ap. J.*, **242**, 1226.  
 Basko, M. M., and Sunyaev, R. A. 1976, *M.N.R.A.S.*, **175**, 395.  
 Baym, G., and Pethick, C. J. 1979, *Ann. Rev. Astr. Ap.*, **17**, 415.  
 Baym, G., Pethick, C. J., and Sutherland, P. G. 1971, *Ap. J.*, **170**, 299.  
 Clayton, D. D. 1968, *Principles of Stellar Evolution and Nucleosynthesis* (New York: McGraw-Hill).  
 Cominsky, L. 1981, Ph.D. thesis, Massachusetts Institute of Technology.  
 Czerny, M., and Jaroszyński, M. 1980, *Acta Astr.*, **30**, 157.  
 Ergma, E. V., and Tutukov, A. V. 1980, *Astr. Ap.*, **84**, 123.  
 Fowler, W. A., Caughlan, G. R., and Zimmerman, B. A. 1975, *Ann. Rev. Astr. Ap.*, **13**, 69.  
 Fryxell, B. A., and Woosley, S. E. 1981, *Ap. J.*, submitted.  
 Fujimoto, M., Hanawa, T., and Miyaji, S. 1981, *Ap. J.*, **247**, 267.  
 Fuller, G. M., Fowler, W. A., and Newman, M. J. 1981, preprints OAP-620 and OAP-621, Kellogg Radiation Laboratory, California Institute of Technology.  
 Giannone, P., and Weigert, A. 1967, *Zs. f. Ap.*, **67**, 41.  
 Glen, G., and Sutherland, P. 1980, *Ap. J.*, **239**, 671.  
 Goldman, Y. 1979, *Astr. Ap.*, **78**, L15.  
 Grindlay, J. E., and Hertz, P. 1981, preprint 1484, Harvard-Smithsonian Center for Astrophysics.  
 Grindlay, J. E., et al. 1980, *Ap. J. (Letters)*, **240**, L121.  
 Hoffman, J. A., Cominsky, L., and Lewin, W. H. G. 1980, *Ap. J. (Letters)*, **240**, L27.  
 Hōshi, R. 1980, preprint.  
 Hoyle, R., and Fowler, W. A. 1965, in *Quasi-Stellar Sources and Gravitational Collapse*, ed. I. Robinson, A. Schild, and E. L. Schucking (Chicago: University of Chicago Press).  
 Inoue, H., et al. 1981, *Ap. J. (Letters)*, **250**, L71.  
 Joss, P. C. 1977, *Nature*, **270**, 310.  
 ———. 1978, *Ap. J. (Letters)*, **225**, L123.  
 ———. 1979, *Comments Ap. Space Sci.*, **8**, 109.  
 Joss, P. C., and Li, F. K. 1980, *Ap. J.*, **238**, 287.  
 Lamb, D. Q., and Lamb, F. K. 1978, *Ap. J.*, **220**, 291.  
 Lamb, F. K., Pethick, C. J., and Pines, D. 1973, *Ap. J.*, **184**, 271.  
 Lederer, C. M., Hollander, J. M., and Perlman, I. 1967, *Table of Isotopes* (6th ed.; New York: Wiley).  
 Lewin, W. H. G., and Joss, P. C. 1981, *Space Sci. Rev.*, **28**, 3.  
 Lewin, W. H. G., et al. 1976, *M.N.R.A.S.*, **177**, 83P.  
 Maraschi, L., and Cavaliere, A. 1977, in *Highlights of Astronomy*, Vol. 4, ed. E. A. Müller (Dordrecht: Reidel), Part I, p. 127.  
 Marshall, H. L. 1981, *Ap. J.*, submitted.  
 Misner, W., Thorne, K. S., and Wheeler, J. A. 1973, *Gravitation* (San Francisco: Freeman).  
 Murakami, T., et al. 1980, *Pub. Astr. Soc. Japan*, **32**, 543.  
 Rakavy, G., Shaviv, G., and Zinamon, Z. 1966, preprint No. OAP-153, Kellogg Radiation Laboratory, California Institute of Technology.  
 ———. 1967, *Ap. J.*, **150**, 131.  
 Salpeter, E. E., and Van Horn, H. M. 1969, *Ap. J.*, **155**, 183.  
 Schwarzschild, M., and Härm, R. 1965, *Ap. J.*, **142**, 855.  
 Sugimoto, D., and Fujimoto, M. Y. 1978, *Pub. Astr. Soc. Japan*, **30**, 467.  
 Swank, J. H., Becker, R. H., Boldt, E. A., Holt, S. S., Pravdo, S. H., and Serlemitsos, P. J. 1977, *Ap. J. (Letters)*, **212**, L73.  
 Taam, R. E. 1980, *Ap. J.*, **241**, 358.  
 ———. 1981a, *Ap. J.*, **247**, 257.  
 ———. 1981b, private communication.  
 Taam, R. E., and Picklum, R. E. 1978, *Ap. J.*, **224**, 210.  
 ———. 1979, *Ap. J.*, **233**, 327.  
 Thorne, K. S. 1977, *Ap. J.*, **212**, 825.  
 Tsuruta, S. 1979, *Phys. Reports*, **56**, 237.  
 van Paradijs, J. 1979, *Ap. J.*, **234**, 609.  
 Van Riper, K. A., and Lamb, D. Q. 1981, *Ap. J. (Letters)*, **244**, L13.  
 Wagoner, R. V. 1969, *Ap. J. Suppl.*, **18**, 247.  
 Wagoner, R. V., Fowler, W. A., and Hoyle, F. 1967, *Ap. J.*, **148**, 3.  
 Wallace, R. K., and Woosley, S. E. 1981, *Ap. J. Suppl.*, **45**, 389.  
 Wallace, R. K., Woosley, S. E., and Weaver, T. A. 1981, *Ap. J.*, submitted.  
 Woosley, S. E., Fowler, W. A., Holmes, J. A., and Zimmerman, B. A. 1975, preprint OAP-422, Kellogg Radiation Laboratory, California Institute of Technology.  
 Woosley, S. E., and Taam, R. E. 1976, *Nature*, **263**, 101.  
 Woosley, S. E., and Wallace, R. K. 1979, private communication.  
 ———. 1981, *Ap. J.*, submitted.

SERPIL AYASLI and PAUL C. JOSS: Room 6-203, Massachusetts Institute of Technology, Cambridge, MA 02139